Master degree in Mathematical Engineering – Advanced Scientific Computing

Internship report entitled

Energy Representation of Systems Described by Partial Differential Equations (PDEs) – Application to Electromagnetic Phenomena –

Kevin AYIVI

April 2nd 2024 – September 30th 2024

Tutors:

Baptiste TRAJIN
Olivier PANTALE

Université de Technologie de Tarbes
Occitanie Pyrénées
Laboratoire Génie de Production

Nouredine MELAB
Olivier GOUBET

Université de Lille

Presentation September 6th 2024

Acknowledgments

I would first like to thank my supervisors Olivier Pantale and Baptiste Trajin for their help and guidance. I would also like to thank Majid Khalili Dermani for his guidance and encouragement throughout my internship.

My gratitude also goes to Thomas Rey, who accepted me into this master's program, to the master's supervisors Nouredine Melab and Olivier Goubet, and to the teaching team for the quality of their teaching, which was beneficial during my internship. I can't forget all those who contributed in any way to the success of my resumption of study, which is the subject of this report.

I would also like to thank my family and friends who have supported me during this year of training. Last but not least, I'd like to thank the members of the LGP, and in particular those of the LGP Open-Space, for their welcome and friendship, which have been a welcome part of this adventure.

Kevin AYIVI

Abstarct

Magnetic materials are usually modeled either globally at component level, or locally at the level of electromagnetic interactions. The weaknesses of these two methods lie in their failure to take into account the multiphysics and dynamics of the system. To overcome these weaknesses, the bond graph is a good approach, as it takes into account the complexity involved in modeling such a system. However, the problem with bond graph models applied to systems described by PDEs is linked to the discretization of space achieved through the meshing technique. To overcome this problem, the choice of numerical method for solving PDEs is crucial. The main objective of this study is to develop a comprehensive model that integrates the finite volume method with the bond graph approach to accurately simulate the macroscopic and microscopic behavior of electromagnetic systems. Through the development of a numerical twin of an electromagnetic coupling system, we explored various modeling techniques and mathematical formulations to capture the complex dynamics of energy transfer.

Key words

- Energy representation

- Electromagnetism

- Partial differential equations

- Maxwell's equations

- Finite volume method

- Bond graph

- Digital twin

Contents

1. Introduction

In view of global warming, the energy transition is driving us to design energy-efficient, low-carbon mobility systems. This improvement in efficiency requires the use of advanced electrical energy conversion structures based on magnetic coupling materials. These materials can be modeled either macroscopically, on the scale of the magnetic component, or locally, using finite element method modeling. However, these two methods do not fully take into account the complexity of these materials. Work at LGP has shown that bond graph model provide a dynamic representation of multiphysical systems, combining macroscopic and microscopic characteristics. However, bond graph modeling of systems described by PDEs is limited by the discretization of space. The finite volume method, which is perfectly suited to conservative phenomena, requires mesh control for diffusive phenomena.

This work is part of a global project to optimize transformers by minimizing hysteresis losses. Hysteresis losses reduce the transformer's overall efficiency by converting part of the electrical energy into useless heat, rather than into useful transferred energy. In this respect, our problem is a low-frequency one.

This study focuses only on electrical and magnetic aspects, without taking into account thermal or mechanical effects. It is crucial for understanding and optimizing transformer operation from an electrical point of view, including winding sizing, core design, and assessment of Joule and hysteresis losses.

The aim of this internship is therefore to overcome the weaknesses of the finite volume method by using unstructured meshes to represent phenomena accurately, while keeping the final algorithmic complexity under control. However, the complexity of this work lies in the coupling of the finite volume method with the bond graph approach to energy modeling, enabling macroscopic and microscopic scales to be brought together.

After a review of the basic concepts required for our study, we'll focus on obtaining a complete physical digital twin of an electromagnetic coupling system, from the geometry of the material and its macroscopic magnetic properties to the equational system used to describe its local dynamics, including a representation in the form of energy transfer.

2. Internship context

2.1 Université de Technologies de Tarbes Occitanie Pyrénées (UTTOP)

UTTOP was established in November 2023 as a result of the merger between the *École Nationale d'Ingénieurs de Tarbes (ENIT)* and the *Institut Universitaire de Technologies (IUT) of Tarbes*, part of *University of Toulouse III - Paul Sabatier*. It thus becomes the fourth *University of Technology*, alongside those of *Belfort-Montbéliard (UTBM), Troyes (UTT), and Compiègne (UTC)*. Its goal is to unite the key players in education, research, and innovation by creating a technological institution of type known as *Établissement public à caractère scientifique, culturel et professionnel (EPSCP)*.

Established in 1970, the IUT of Tarbes educates 1,500 students primarily in *university bachelor's degrees in technology (BUT)* and *professional bachelor's degrees (LP)*. These programs are distributed across eight academic departments.

Founded in 1963, *ENIT* is one of the 204 French engineering schools accredited (as of September 1, 2020) to award an engineering degree. It trains generalist engineers in mechanical engineering and industrial engineering capable of designing, implementing, and managing industrial systems and production equipment. In 1989, it established a research laboratory : *Laboratoire Génie de Production (LGP)*.

2.2 Laboratoire Génie de Production (LGP)

LGP is a multidisciplinary laboratory whose research falls within the field of systems science and engineering. It is structured into two scientific departments, each composed of five research groups:

➤ Scientific Department of Mechanics-Materials-Processes

➥ **D^{2}PAM** : New Design-Process-Durability Links in SLM Additive Manufacturing

➥ **FIRST** : Fatigue and Interfaces for Reliable and Durable Thermoplastics

➥ **IMPACT** : Interfaces Materials, Polymers, Assemblies, Composites, and Textiles

➥ **M^{2}SD** : Metallurgy Mechanics Structures and Damage

➥ **TM^{2}P** : Tribology, Materials & Process Mechanics

➢ Scientific Department of Systems

➥ **e-ACE**[2] : Efficiency of Electrical Energy Conversion Systems
➥ **ICE** : Knowledge and Experience Engineering for Process, Systems, and Organizational Improvement
➥ **MAVRICS** : Mechatronics, Automation, Virtual Reality, and Robotics for System Interaction
➥ **PICS** : Planning, Interoperability, and Coordination for System Dynamics
➥ **PRiSM** : Prognostics & Risk Management for System Resilience

Additionally, there are two cross-disciplinary axes:

➢ **PAMS** : Intelligent Additive Processes, from Matter to System

➢ **JN** : Digital Twin

LGP also benefits from various technology transfer platforms, which allow it to provide concrete solutions to the problems faced by companies.

2.3   My supervisors

2.3.1   Olivier Pantalé

Olivier Pantalé obtained an engineering degree from ENIT in 1992 and a Ph.D. in Mechanics from the University of Bordeaux I in 1996. In 2005, he earned his Habilitation to Supervise Research from the *Institut National Polytechnique* of Toulouse. He is currently a full professor of mechanics at UTTOP and a member of the M^{2}SD research group at LGP. His work in numerical mechanics and materials science has led to several publications and membership in the European association DYMAT for the study of the dynamic behavior of materials, among others.

His research focuses on numerical modeling of the behavior of materials subjected to large deformations, high strain rates, and high temperatures, with applications in metal forming processes. He has developed expertise in the development and use of nonlinear finite element codes, which he teaches at ENIT and ISAE-SUPAERO in Toulouse.

2.3.2   Baptiste Trajin

Baptiste Trajin obtained an engineering degree in electrotechnics and automation from the *Ecole Nationale Supérieure d'Electrotechnique, d'Electronique, d'Informatique, d'Hydraulique et des Telecommunications* of Toulouse in 2006, and a Ph.D. in Electrical Engineering in 2009 from the *Institut National Polytechnique* of Toulouse. He is currently an associate professor in electrotechnology at ENIT and a member of the e-ACE^2 research group at LGP.

His research area is the diagnosis of electromechanical systems. He is currently working on the modeling, estimation, and diagnosis of multiphysical systems such as mechatronic systems and power electronic modules.

He supervises Majid Khalili Dermani thesis, whose work has led this internship.

Majid Khalili Dermani

Holding a master's degree in Electrical Engineering from the University of Grenoble-Alpes, Majid is preparing a thesis with INP Toulouse. He is part of the e-ACE^2 research group at LGP. Entitled "Modeling Electromagnetic Couplings through a Systemic Approach for the Energy Efficiency of Static Converters", his thesis revolves around two main and complementary activities:

➢ Local energetic representation of electromagnetic phenomena governed by second-order PDEs (Maxwell's equations) using bond graph.

➢ Considering the intrinsic local physical properties of the material to reproduce macroscopic behaviors such as hysteresis.

This internship is part of the first activity, which will use a finite volume approach for energetic representation.

This work is broadly part of a railway traction system optimization project.

3.   Background

To understand the framework of this project, we will introduce the basic tools and concepts necessary for comprehension.

3.1   Electrical circuits [10]

Electric current, voltage and power

Electric charge is a property of matter that generates an electromagnetic field. It is a scalar quantity, additive and conservative. The movement of these charges within the material leads to the creation of an *electric current*. *Electric current* is thus defined as the flow of electric charge through a surface. It is measured in *Amperes (A)*.

In an electrical circuit, some wires intersect at a point. The *Kirchhoff's current law (KCL)* states the algebraic sum of currents in a network of conductors meeting at a point is zero.
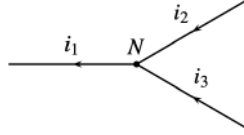

$$i_1 = i_2 + i_3 \qquad (3.1)$$

Figure 3.1: Illustration of KCL

In an electrical circuit, the pressure from the power source that induces the electric current is called *voltage*. It is measured in *Volts (V)*. It is also defined as the difference in electric potential between two points; with electric potential being the amount work required to move a unit charge from a reference point to a specific point in an electric field.

The directed sum of the voltages around any closed loop (without branches) is zero. This law is called *Kirchhoff's voltage law (KVL)*.
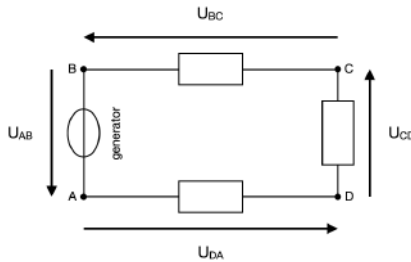
$$U_{AB} + U_{BC} + U_{CD} + U_{DA} = 0 \quad (3.2)$$

Figure 3.2: Illustration of KVL

In summary, voltage is the electric effort that drives the electric flow (current).

Power is the amount of energy transferred or consumed by a components per unit of time. The instantaneous power $\mathscr{P}$ exchanged is calculated by :

$$\mathscr{P}(t) \;=\; u(t) \times i(t) \tag{3.3}$$

Components

An electrical circuit is composed of two types of components.

➤ Active component (Generator) induces the electric voltage and current in the system.

➤ Passive component which cannot generate current itself. If it is not subjected to any voltage, no current flows through it. The three most commonly used passive components are:

➥ *Resistor* implements electrical resistance as a circuit element. (e.g., to reduce current flow)

$$u(t) \;=\; R\, i(t) \qquad (3.4) \qquad \text{R is called resistance.}$$

➥ *Capacitor* stores electrical energy by accumulating electric charges on two closely spaced surfaces that are insulated from each other.

$$i(t) \;=\; C\,\frac{d\,u(t)}{dt} \qquad (3.5) \qquad \text{C is called capacitance.}$$

➥ *Inductor* stores energy in a magnetic field when electric current flows through it.

$$u(t) \;=\; L\,\frac{d\,i(t)}{dt} \qquad (3.6) \qquad \text{L is called inductance.}$$

3.2   Bond Graph [2]

Definitions

Bond Graph is a graphical language for representing power transfers within a system. It is based on the notion of analogy and assumes parameters localized in the system. It explicitly shows cause-and-effect relationships (causality), which allows for the systematic construction of "classical" mathematical models. Bond Graph is used in different physical domain.

In the overall system composed of two subsystems A and B, there is energy conservation and power continuity. The exchanged power $\mathscr{P}$ is expressed as the product of two complementary variables. Independently of the considered domain, these variables are called "generalized variables" of effort (e) and flow (f).

$$\mathscr{P} \;=\; e \times f \tag{3.7}$$

The power transfer between the two subsystems is represented by a half-arrow, corresponding to the "bond" of the bond graph. By convention, the flow is always represented on half-row side.

Figure 3.3: Bond Graph illustration

The energy is calculated by integrating power with respect to time.

$$\mathscr{E}(t) \;=\; \int_0^t e(\tau)\, f(\tau)\, d\tau \;+\; \mathscr{E}(0) \tag{3.8}$$

We also get two variables called « generalized momentum » (p) and « generalized displacement » (q).

$$p(t) \;=\; \int_0^t e(\tau)\, d\tau \;+\; p(0) \tag{3.9}$$

$$q(t) \;=\; \int_0^t f(\tau)\, d\tau \;+\; q(0) \tag{3.10}$$

Causality

When two subsystems A and B interact and exchange power, two situations are possible.

1. *A* applies an effort *e* to *B*, which reacts by sending a flow $f \;=\; \Psi_B(e)$ to *A*.

2. *A* sends a flow *f* to *B*, which reacts with an effort $e \;=\; \lambda_B(f)$ to *A*.

To represent these cause-and-effect relationships on a bond graph model, a « causal stroke » is placed perpendicular to each bond, following this convention.

- The causal stroke is placed near (respectively far from) the element for which the effort (respectively the flow) is given.

- The position of the causal stroke is independent of the direction of the half-arrow.
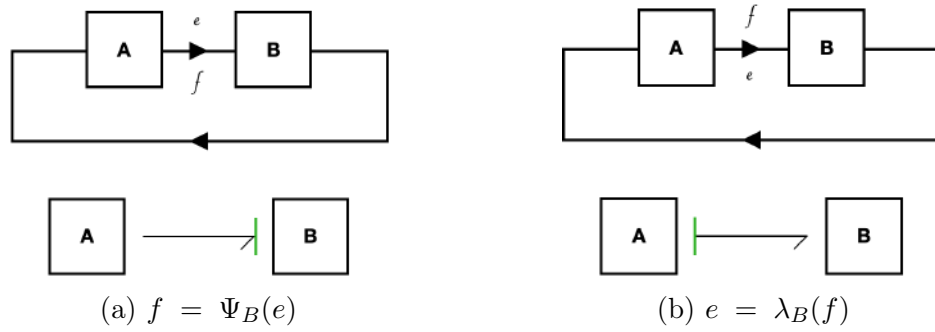
(a) $f = \Psi_B(e)$ (b) $e = \lambda_B(f)$

Figure 3.4: Causality illustration

Elements

We distinguish three types of elements for the bond graph.

➤ Active elements

   ➥ Sources Se and Sf supply power to the system.

Figure 3.5: Source representation

   ➥ Detectors indicate the presence of a sensor or measuring instrument (Not use in our projet)

➤ Passive elements. We can distinguish two types.

   ➥ 1-port passive elements

      ⇨ R element is used to model any physical phenomenon linking the effort variable to the flow variable. (2 types of representation and characteristic law)

Figure 3.6: First representation

$$e = Rf \qquad (3.11)$$

Figure 3.7: Second representation

$$f = \frac{1}{R}e \qquad (3.12)$$

      ⇨ C element is used to model any physical phenomenon linking the effort variable to the displacement variable.

Figure 3.8: C representation

$$e(t) = \Psi_C^{-1}\left(\int_t f(\tau)\, d\tau\right) \qquad (3.13)$$

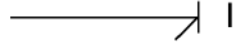⟿ I element is used to model any physical phenomenon linking the flux variable to the moment variable.

Figure 3.9: I representation

$$f(t) \;=\; \Psi_I^{-1}\left(\int_t e(\tau)\,d\tau\right) \quad (3.14)$$

➥ Multiport passive elements help to represent phenomena that cannot be represented using independent 1-port elements. (e.g., winding of 3 inductors)

Figure 3.10: Multiport element representation

➢ Junction elements. We distinguish four types.

➥ 0 is used to couple elements subject to the same effort. The 0-junction is characterize by equality of effort for all links having an end on the junction and algebraic sum of the powers equals zero. Only one causal stroke is near the 0-junction.
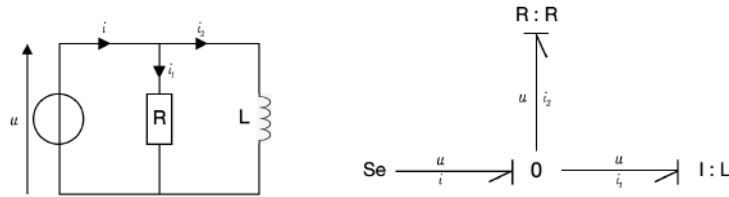

Figure 3.11: KCL Bond Graph

➥ 1 is used to couple elements traversed by the same flow. The 1-junction is characterize by equality of flux for all links having an end on the junction and algebraic sum of the powers equals zero. Only one causal stroke is far the 1-junction.
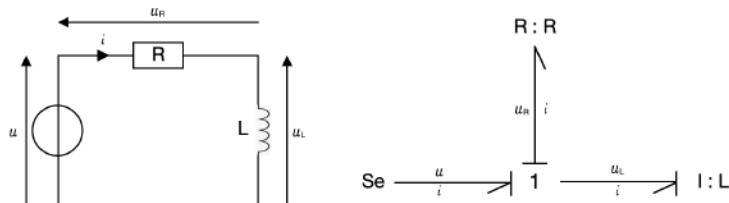

Figure 3.12: KVL Bond Graph

➥ TF behaves as a transformer. There is a relationship between flow in and flow out / effort in and effort out without power loss.

➥ GY behaves as a gyrator. There is a relationship between effort in and flow out / flow in and effort out without power loss.

Note : In the context of this study, we choose to represent the characteristic laws in their integral forms, but it is entirely possible to represent them in their differential forms. The characteristic laws will therefore be of the same form (for I and C) as those stated for electrical components (inductor and capacitor, respectively).

On the basis of numerical arguments, the integral form is preferred, due to the fact that numerical differentiation amplifies numerical noise. The integral form allows the use of an initial condition, which is a physically relevant property that clearly illustrates the statement that integration "exist" in nature. Differentiation with reference to time requires information about future states, whereas integration with reference to time does not.

3.3   Electromagnetic

When a conductor is traversed by an electric current, a magnetic force is generated. Electromagnetism is the study of interactions between electrically charged particles, using the concept of the electromagnetic field. Electromagnetic force is one of the four fundamental forces of nature. An electromagnetic field is a spatiotemporal representation of the electromagnetic force exerted by charged particles. This field results from the combination of an electric wave and a magnetic wave, which propagate at the speed of light.

Notations

- $\nabla \times$: curl operator

- $\nabla \cdot$: divergence operator

- $\partial_t = \dfrac{\partial}{\partial t}$

Définitions

- *Electric field* $\mathbf{E}$ is a field created by the attraction and repulsion of electric charges. It is expressed in volts per meter (V/m) and varies with time.

- *Magnetic field* $\mathbf{H}$ is a field resulting from the movement of charges. It is expressed in amperes per meter (A/m) and varies with time.

- [6]*Current density* $\mathbf{J}$ refers to the electric current per unit area. At low frequencies, its distribution occurs throughout the entire volume of the conductor; however, at high frequencies, it tends to move away from the center of the conductor towards its periphery. This is known as the skin effect. $\mathbf{J}$ is the sum of three current densities. It is expressed in amperes per square meter (A/m^2) and varies with time.

  ➥ *Conduction current* $\mathbf{J}_\sigma$ is the flow of free charges through a conductor.

  $$\mathbf{J}_\sigma \ = \ \sigma \mathbf{E} \tag{3.15}$$

  ➥ *Convection current* $\mathbf{J}_s$ is the flow of free charges through an insulator. For convection current to exist, the insulators must be charged.

➥ *Displacement current* $\mathbf{J}_D$ is due to bound charges. There exists a short-lived net movement of charge as a material changes its state of polarization.

$$\mathbf{J}_D \;=\; \varepsilon \, \partial_t \mathbf{E} \tag{3.16}$$

- *Electric charge density* ρ refers to the amount of electric charge per unit volume. It is expressed in coulombs per cubic meter (C/m^3).

- *Magnetic permeability* μ is the property of a material to modify a magnetic field. It is expressed in henries per meter (H/m). Permeability in vacuum is denoted μ_0 ($\mu_0 = 4 \cdot \pi \cdot 10^{-7} \; H/m$).

- *Electric permittivity* ε is the response of a material when subjected to an electric field. It is expressed in farads per meter (F/m). Permittivity in vacuum is denoted ε_0 ($\varepsilon_0 \simeq 8.85 \cdot 10^{-12} \; F/m$).

- *Electrical conductivity* σ characterizes the property of a material that allows the passage of electric current. It is expressed in siemens per meter (S/m)

Maxwell's equations

The study, design, and optimization of an electromagnetic (EM) system often require the implementation of mathematical models that feature Maxwell's equations, which are capable of representing and characterizing the system's behavior.

$$\begin{cases} \nabla \cdot \mathbf{E} \;=\; \frac{\rho}{\varepsilon} & \text{Gauss's law for electricity} \\[2mm] \nabla \cdot \mu\mathbf{H} \;=\; 0 & \text{Gauss's law for magnetism} \\[2mm] \nabla \times \mathbf{E} \;=\; -\mu \, \partial_t \mathbf{H} & \text{Faraday's law} \\[2mm] \nabla \times \mathbf{H} \;=\; \mathbf{J} & \text{Ampere's law} \end{cases} \tag{3.17}$$

3.4 State-space representation

State-space representation is a mathematical framework used to model and analyze dynamic systems. It is a powerful and versatile technique for the representation, analysis, and control of dynamic systems. It provides a structured and systematic view of the internal dynamics, thereby facilitating numerical simulation.

State of a system is the vector containing the information necessary to determine the future state of the system, taking into account its initial conditions and inputs. The *inputs* represent the external variables that influence the system. This implies that there are *outputs*, which are the system's response variables resulting from the *inputs*.

$$\begin{cases} \dot{x}(t) \;=\; Ax(t) \;+\; Bu(t) & \text{State Equation} \\[2mm] y(t) \;=\; Cx(t) \;+\; Du(t) & \text{Output Equation} \end{cases} \tag{3.18}$$

Note : We only obtain the output equation for finite-dimensional linear systems.

- $x(t)$: state vector

- $y(t)$: output vector

- $u(t)$: input vector

- A : state matrix (describing the system's dynamics)

- B : input matrix (describing how inputs affect the states)

- C : output matrix (describing how states affect the outputs)

- D : feedthrough matrix (describing the direct effect of inputs on outputs)

State-space representation is used to simulate bond graphs because it provides a uniform and rigorous description of dynamic systems, (just as bond graph does) for the discipline of physics. It captures the dynamic behavior of systems through state variables, facilitating the numerical resolution of the associated differential equations. In bond graph modeling and the associated state-space representation, the system state $x(t)$ is defined by the forces and flows of the energy storage elements (such as C and I), while the inputs $u(t)$ correspond to the forces and flows imposed by external sources (such as Se and Sf). Obviously, state space representation is able to describe variables along time using a numerical integration algorithm such as *Euler* or *Runge-Kutta* methods.

3.5   Train traction system [1]

Electric train traction is the result of three physical subsystems. It begins upstream with the general electrical power network, which provides the train with the electrical energy it needs to operate, and ends downstream with the train's mechanical movement, driven by the wheels. Between these two systems lies the train's traction system, which transforms the electrical energy received into mechanical energy. There are two types of traction system (direct current power source system – DC – and alternative current power source system – AC –), and they are made up of 4 main parts.

- ➢ Pantograph collects the electrical energy (AC or DC) supplied by the power network from the catenary.

- ➢ Transformer adapts AC voltage level.

- ➢ Converters perform AC/DC conversion.

- ➢ Motors power the kinematics for traction.

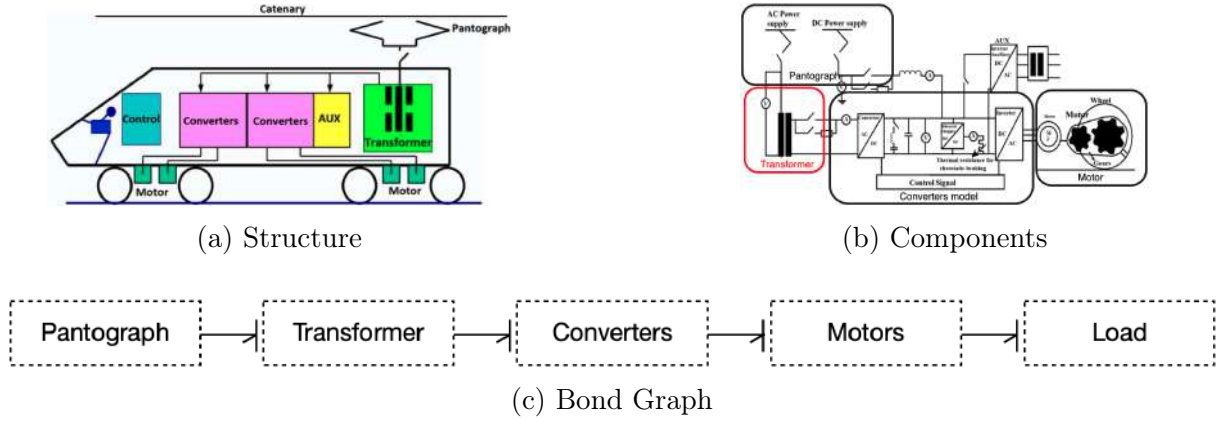(a) Structure

(b) Components

(c) Bond Graph

Figure 3.13: Train traction system

3.6 Project

Previous work at LGP [1] on the real-time simulation of electrical models of traction subsystems has shown that it is important to take into account the models of non-linear subsystems of the train traction system, such as the transformer. Modeling this electrical energy conversion structure using magnetic coupling materials requires consideration of its dynamic and multiphysics aspects.
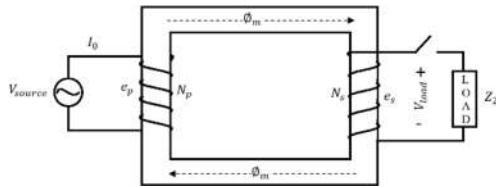

Figure 3.14: Ideal transformer with primary and secondary windings
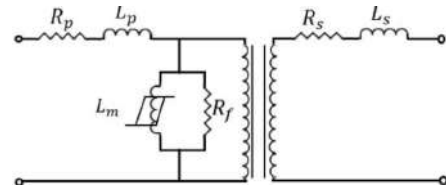

Figure 3.15: Equivalent circuit of single-phase power transformer

Bond graph, although well-suited to its complex representation, encounters limitations due to space discretization. For this, the choice of the classical numerical method for solving systems described by PDEs is essential. PDE is a continuous, infinite-dimensional description of a system, but for numerical simulation we need to move from the continuous to the discrete domain. To do this, we use classical mathematical methods for solving PDEs to discretize our PDE problem. Majid's thesis work demonstrated the advantages and disadvantages of coupling the bond graph with the finite difference method (FDM) and the finite element method (FEM).

FDM, although effective for dealing with coupled electromagnetic problems, involve the use of a very fine mesh, increasing the cost of resolution [7]. FEM, which are more suitable for complex geometries, are unable to handle the dual variables of electromagnetics in a single numerical resolution [4].

The aim of this work is therefore to couple finite volume method (FVM) for discretizing the PDEs governing electromagnetism with the bond graph. This will enable us to obtain

a multi-fidelity model describing both the multiphysics and dynamics of a transformer.

In the rest of this report, we'll start by presenting the work on FDM in dimension 1, which is simpler to understand and has produced good results. We will then carry out a study analogous to that of FDM, but for FVM in different spatial dimensions.

4. State of art [7]

4.1 EM fields power

To model electromagnetic phenomena using the bond graph, one need to define electromagnetic power. As we saw earlier, the train traction system involves 3 physical phenomena: electricity, mechanics and electromagnetism. One therefore need to choose global effort and flux variables that are consistent with other physical phenomena and guarantee continuity in the modeling of power transfers.

Table 4.1: Elerticity and mechanics power representation

	Effort	Flow
Electrical	Voltage (V)	Current (A)
Mechanical	Force (N)	Velocity (m/s)

In EM systems, the calculation of power is facilitated through the Poynting's vector represented as :

$$\mathbf{\Pi} \;=\; \mathbf{E} \times \mathbf{H} \tag{4.1}$$

For the sake of clarity and consistency with electrical power, we choose $\mathbf{E}$ (V/m) as the effort variable and $\mathbf{H}$ (A/m) as the flux variable.

4.2 System under study

4.2.1 Infinitely long wire

The concept of an infinite long wire is used in electromagnetism to simplify the analysis of electric and magnetic fields produced by an electric current. An infinite long wire is a theoretical physical model that assumes a very thin, infinitely long conductor wire, located in a non-magnetic domain, with a constant electric current flowing through it. This idealization simplifies calculations and helps us better understand certain electromagnetic phenomena. Given the geometry of the model, the use of a cylindrical coordinate system with basis vectors (e_r, e_φ, e_z), proves to be the most appropriate.
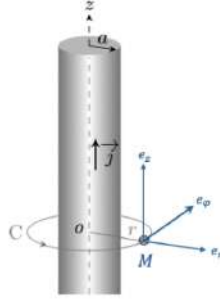
Figure 4.1: Infinitely long wire and associated cylindrical coordinate system

4.2.2 System modeling

To observe and analyze the magnetic fields of the previous system, one need to write the last two Maxwell equations (Ampère and Faraday) in cylindrical coordinates.

| Faraday's law | Ampere's law |

$$\begin{cases} \dfrac{1}{r}\dfrac{\partial \mathbf{E}_z}{\partial \varphi} - \dfrac{\partial \mathbf{E}_\varphi}{\partial z} = -\mu\,\dfrac{\partial \mathbf{H}_r}{\partial t} \\[2mm] \dfrac{\partial \mathbf{E}_r}{\partial z} - \dfrac{\partial \mathbf{E}_z}{\partial r} = -\mu\,\dfrac{\partial \mathbf{H}_\varphi}{\partial t} \\[2mm] \dfrac{1}{r}\left[\dfrac{\partial}{\partial r}r\mathbf{E}_\varphi - \dfrac{\partial \mathbf{E}_r}{\partial \varphi}\right] = -\mu\,\dfrac{\partial \mathbf{H}_z}{\partial t} \end{cases} \tag{4.2}$$

$$\begin{cases} \dfrac{1}{r}\dfrac{\partial \mathbf{H}_z}{\partial \varphi} - \dfrac{\partial \mathbf{H}_\varphi}{\partial z} = \sigma\mathbf{E}_r + \mathbf{J}_{\mathbf{s}r} + \varepsilon\dfrac{\partial \mathbf{E}_r}{\partial t} \\[2mm] \dfrac{\partial \mathbf{H}_r}{\partial z} - \dfrac{\partial \mathbf{H}_z}{\partial r} = \sigma\mathbf{E}_\varphi + \mathbf{J}_{\mathbf{s}\varphi} + \varepsilon\dfrac{\partial \mathbf{E}_\varphi}{\partial t} \\[2mm] \dfrac{1}{r}\left[\dfrac{\partial}{\partial r}r\mathbf{H}_\varphi - \dfrac{\partial \mathbf{H}_r}{\partial \varphi}\right] = \sigma\mathbf{E}_z + \mathbf{J}_{\mathbf{s}z} + \varepsilon\dfrac{\partial \mathbf{E}_z}{\partial t} \end{cases} \tag{4.3}$$

Given an infinite wire running along the z axis and carrying a uniform current $\mathbf{J}$. The right-hand rule indicates that the electric field $\mathbf{E}$ will be in the z direction due to the uniform current $\mathbf{J}$ and magnetic field $\mathbf{H}$ will be in the direction of φ.
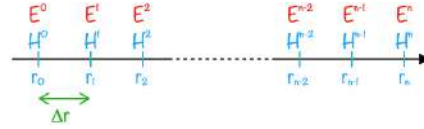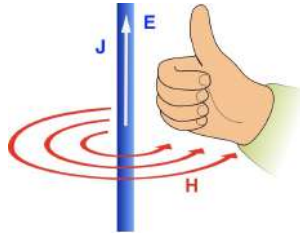

Figure 4.2: Ampère's right-hand grip rule

Moreover, as the insulator is not charged, there is no convection current ($\mathbf{J}_s = 0$). Applying these simplifications to (4.2) and (4.3), we obtain

$$\begin{cases} \dfrac{\partial \mathbf{E}_z}{\partial r} = \mu\,\dfrac{\partial \mathbf{H}_\varphi}{\partial t} \\[3mm] \dfrac{1}{r}\,\mathbf{H}_\varphi + \dfrac{\partial \mathbf{H}_\varphi}{\partial r} = \sigma\mathbf{E}_z + \varepsilon\dfrac{\partial \mathbf{E}_z}{\partial t} \end{cases} \tag{4.4}$$

For FDM modeling, we use non-staggered grid, an alternative to Yee's algorithm. This defines a space staggered grid for calculating the two fields. Electric field and magnetic field are calculated in the vertex of the control volumes. The scheme in (4.4) give us :

Figure 4.3: Non-staggered grid along r direction

$$
\begin{cases}
\dfrac{\mathbf{E}_z^{i+1} - \mathbf{E}_z^i}{\Delta r} = \mu \dfrac{\partial \mathbf{H}_\varphi^i}{\partial t} \\[3mm]
\dfrac{1}{r_i}\mathbf{H}_\varphi^i + \dfrac{\mathbf{H}_\varphi^{i+1} - \mathbf{H}_\varphi^i}{\Delta r} = \sigma \mathbf{E}_z^i + \varepsilon \dfrac{\partial \mathbf{E}_z^i}{\partial t}
\end{cases}
\tag{4.5}
$$

To simulate the Bond Graph, we use the state representation. In our case, only the first equation of (3.18) (state equation) is required.

$$
\dot{x}(t) = Ax(t) + Bu(t) \tag{4.6}
$$

$$
\begin{cases}
x(t) = (E_z^i(t),\ H_\varphi^i(t)) \\[2mm]
u(t) = (J_\sigma^i(t),\ H_\varphi^0(t),\ H_\varphi^{+\infty}(t))
\end{cases}
$$

4.2.3 Magnetostatic analytic solution

In this study, the time dependency of variables is out of concern i.e. variables are constant along time. To validate the model, we compare it with its magnetostatic analytic solution. This involves calculating the magnetic field using the integral Ampere's law :

$$
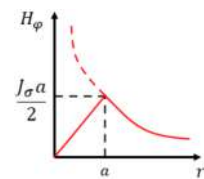\oint_C \mu \mathbf{H}\, dl = \iint_S \mathbf{J}\, ds \tag{4.7}
$$

- $\mathbf{J} = \begin{cases} \mathbf{J}_\sigma e_z & \text{In wire} \\ 0 & \text{In air} \end{cases}$

- $\oint_C \mu \mathbf{H}\, dl = 2\pi r \mu \mathbf{H}_\varphi(r)$

We obtain :

$$
\begin{cases}
\mathbf{H}_\varphi(r) = \dfrac{\mathbf{J}_\sigma\, r}{2} & \text{In wire} \\[3mm]
\mathbf{H}_\varphi(r) = \dfrac{\mathbf{J}_\sigma\, a^2}{2} & \text{In air}
\end{cases}
\qquad a \ : \ \text{wire radius} \tag{4.8}
$$
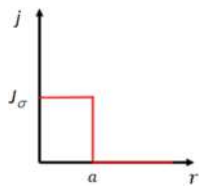
(a) Current density

(b) Magnetic field

Figure 4.4: Magnetostatic analytic solution

4.3 Results

4.3.1 Bond Graph

From (4.5), we get

➢ Faraday's law $\Rightarrow$ $\quad \mathbf{H}_\varphi^i = \dfrac{1}{\mu \Delta r} \displaystyle\int_t \mathbf{E}_z^{i+1} - \mathbf{E}_z^i \, d\tau \Rightarrow \quad I$ and 1-junction

➢ Ampere's law $\Rightarrow$ $\quad \mathbf{H}_\varphi^{i+1} - \mathbf{H}_\varphi^i = \sigma \Delta r \mathbf{E}_z^i + \varepsilon \Delta r \dfrac{\partial \mathbf{E}_z^i}{\partial t} - \dfrac{\Delta r}{r_i} \mathbf{H}_\varphi^i \Rightarrow \quad$ 0-junction

➥ In wire $\quad \varepsilon \dfrac{\partial \mathbf{E}_z}{\partial t} = 0 \Rightarrow \quad MSf$ (modulated Sf) $\qquad (Sf$, when $i = 0)$

➥ In air $\quad \varepsilon \dfrac{\partial \mathbf{E}_z}{\partial t} \neq 0 \Rightarrow \quad R, \, C, \, MSf$
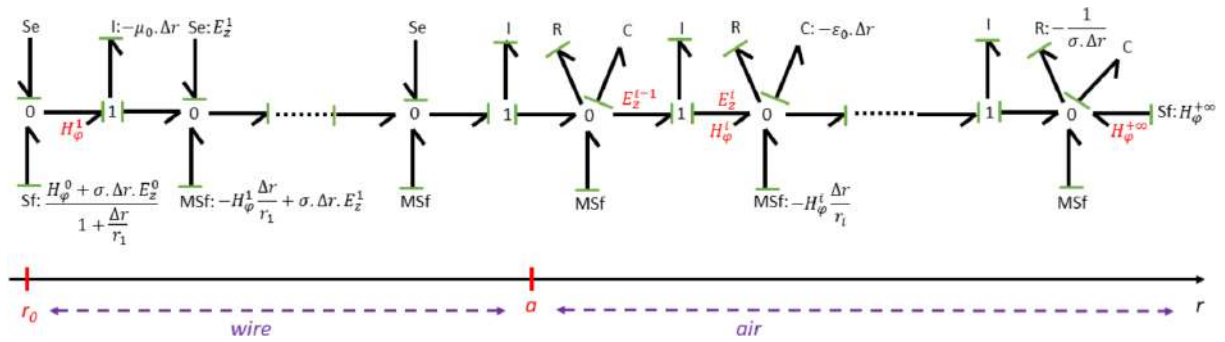

Figure 4.5: Bond graph representation of 1D discrete Maxwell's equations using FDM
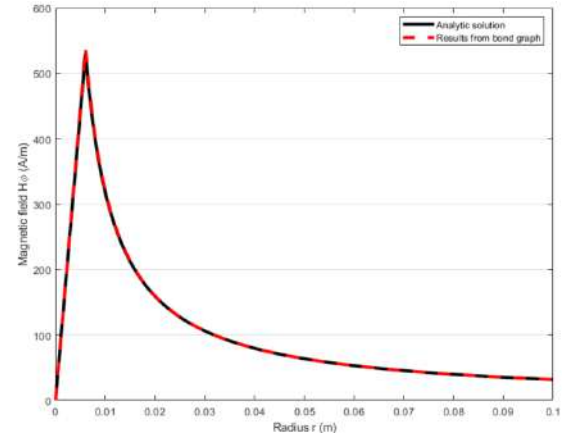
4.3.2 Simulation

Considering an infinitely long wire of radius $a = 6$ mm and a constant discretisation step of $\Delta r = 0.1$ mm, electric and magnetic fields are computed for $0 \leq r \leq 10$ cm using the state space system obtained from bond graph with nonstaggered grid. The results are then compared with those obtained with analytic expressions in (4.8), and depicted in Figure 4.6. Moreover, electric field is also depicted and it can be seen that it is effectively proportional to current density.

In this study, Matlab software is used to solve numerical systems of equations. It can be remarked that other numerical computing software or language, such as Python, could be used with similar results.

Finally, the results obtained in the steady state from bond graph modeling are totally consistent with analytic simulations, exhibiting a maximum relative error of just 1.6%, thereby leading to a clear validation of the proposed methodology for representing coupled magnetic and electric fields.
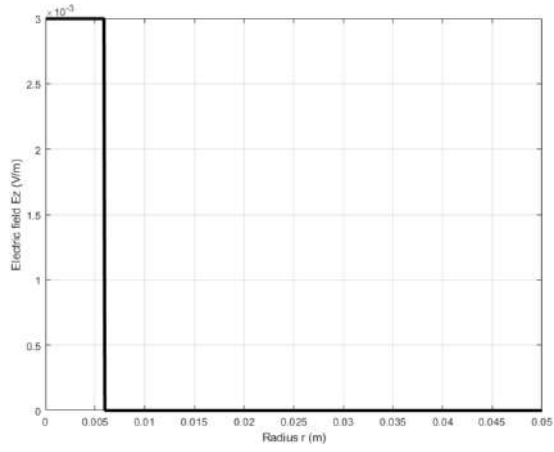
(a) Current density

(b) Magnetic field

Figure 4.6: Simulation results of EM fields in steady state

5.   Methods

The FVM models used during the course are based on the centered method for calculating electric and magnetic fields. The ultimate goal is to find an optimal calculation method using unstructured meshes, and to simplify computation so that **E** and **H** are calculated at the same points.

5.1   FVM vs FDM 1D discrete Maxwell's equations

In this first part, we compare the two methods based on the calculations in the previous section. This is a first approach to testing the consistency of the FVM model.

5.1.1   FVM discretization
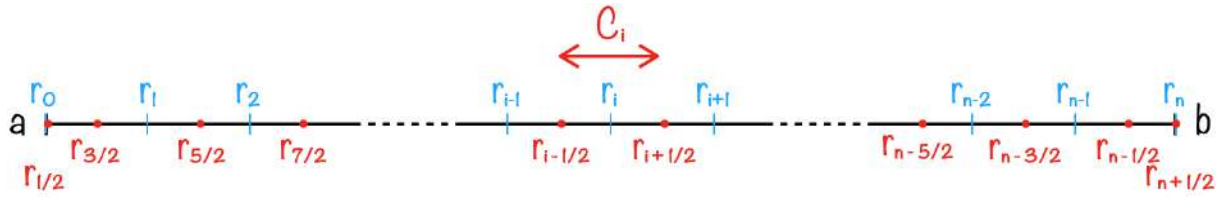
The following regular mesh is used :

Figure 5.1: 1D regular mesh for FVM

- $x_{i+\frac{1}{2}} \in (x_i, \ x_{i+1})$,

- $x_0 = x_{\frac{1}{2}} = a$

- $x_n = x_{n+\frac{1}{2}} = b$

Applied 1D FVM scheme on (4.4) gives for control volume in i :

$$\begin{cases} \displaystyle\int_{x_{i-\frac{1}{2}}}^{x_{i+\frac{1}{2}}} \frac{\partial \mathbf{E}_z}{\partial x}\,dx & = & \displaystyle\int_{x_{i-\frac{1}{2}}}^{x_{i+\frac{1}{2}}} \mu\frac{\partial \mathbf{H}_\varphi}{\partial t} \\[3mm] \displaystyle\int_{x_{i-\frac{1}{2}}}^{x_{i+\frac{1}{2}}} \frac{1}{x}\mathbf{H}_\varphi + \frac{\partial \mathbf{H}_\varphi}{\partial x}\,dx & = & \displaystyle\int_{x_{i-\frac{1}{2}}}^{x_{i+\frac{1}{2}}} \sigma\mathbf{E}_z + \varepsilon\frac{\partial \mathbf{E}_z}{\partial t}\,dx \end{cases} \tag{5.1}$$

$$\Rightarrow \begin{cases} \dfrac{\mathbf{E}_z^{i+\frac{1}{2}} - \mathbf{E}_z^{i-\frac{1}{2}}}{\Delta r} & = & \mu\dfrac{d\mathbf{H}_\varphi^i}{dt} \\[3mm] \dfrac{1}{r_i}\mathbf{H}_\varphi^i + \dfrac{\mathbf{H}_\varphi^{i+\frac{1}{2}} - \mathbf{H}_\varphi^{i-\frac{1}{2}}}{\Delta r} & = & \sigma\mathbf{E}_z^i + \varepsilon\dfrac{d}{dt}\mathbf{E}_z^i \end{cases} \tag{5.2}$$

$$\Delta r = |C_i| \qquad , \qquad |C_i| : \text{length of } C_i$$

There is a consistency problem with (5.2). To resolve this, we use linear interpolation. For comparison with the FDM model, we take the opportunity to place the calculation of **E** and **H** at the same point.

$$\begin{cases} \dfrac{\frac{1}{2}(\mathbf{E}_z^{i+1} - \mathbf{E}_z^i) - \frac{1}{2}(\mathbf{E}_z^i - \mathbf{E}_z^{i-1})}{\Delta r} & = & \mu \dfrac{d\mathbf{H}_\varphi^i}{dt} \\[4mm] \dfrac{1}{r_i}\mathbf{H}_\varphi^i + \dfrac{\frac{1}{2}(\mathbf{H}_\varphi^{i+1} - \mathbf{H}_\varphi^i) - \frac{1}{2}(\mathbf{H}_\varphi^i - \mathbf{H}_\varphi^{i-1})}{\Delta r} & = & \sigma \mathbf{E}_z^i + \varepsilon \dfrac{d}{dt}\mathbf{E}_z^i \end{cases} \tag{5.3}$$

$$\Rightarrow \quad \begin{cases} \dfrac{\mathbf{E}_z^{i-1} - 2\mathbf{E}_z^i + \mathbf{E}_z^{i+1}}{2\Delta r} & = & \mu \dfrac{d\mathbf{H}_\varphi^i}{dt} \\[4mm] \dfrac{1}{r_i}\mathbf{H}_\varphi^i + \dfrac{\mathbf{H}_\varphi^{i-1} - 2\mathbf{H}_\varphi^i + \mathbf{H}_\varphi^{i+1}}{2\Delta r} & = & \sigma \mathbf{E}_z^i + \varepsilon \dfrac{d}{dt}\mathbf{E}_z^i \end{cases} \tag{5.4}$$

5.1.2   Bond Graph with 1D FVM scheme

From (5.2), we get

➤ Faraday's law $\Rightarrow$ $\quad \mathbf{H}_\varphi^i = \dfrac{1}{2\mu\Delta r} \displaystyle\int_t \mathbf{E}_z^{i-1} - 2\mathbf{E}_z^i + \mathbf{E}_z^{i+1} \, d\tau \Rightarrow \quad I$ and 1-junction

➤ Ampere's law $\Rightarrow$ $\quad \mathbf{H}_\varphi^{i-1} - 2\mathbf{H}_\varphi^i + \mathbf{H}_\varphi^{i+1} = 2\sigma\Delta r\mathbf{E}_z^i + 2\varepsilon\Delta r\dfrac{\partial \mathbf{E}_z^i}{\partial t} - \dfrac{2\Delta r}{r_i}\mathbf{H}_\varphi^i$

$\Rightarrow$ $\quad$ 0-junction

➥ In wire $\quad \varepsilon \dfrac{\partial \mathbf{E}_z}{\partial t} = 0 \Rightarrow \quad MSf$

➥ In air $\quad \varepsilon \dfrac{\partial \mathbf{E}_z}{\partial t} \neq 0 \Rightarrow \quad R, \, C, \, MSf$

➥ On boundary, $\mathbf{H} = 0$, Sf on left and MSf on right)

$$\begin{cases} \dfrac{1}{r_i}\mathbf{H}_\varphi^i + \dfrac{\mathbf{H}_\varphi^{i+\frac{1}{2}}}{\frac{\Delta r}{2}} = \sigma\mathbf{E}_z^i + \varepsilon\dfrac{d}{dt}\mathbf{E}_z^i & \text{on left boundary} \\[5mm] \dfrac{1}{r_i}\mathbf{H}_\varphi^i - \dfrac{\mathbf{H}_\varphi^{i-\frac{1}{2}}}{\frac{\Delta r}{2}} = \sigma\mathbf{E}_z^i + \varepsilon\dfrac{d}{dt}\mathbf{E}_z^i & \text{on right boundary} \end{cases} \tag{5.5}$$

Equation (5.4) becomes

$$\begin{cases} \dfrac{1}{r_i}\mathbf{H}_\varphi^i + \dfrac{\mathbf{H}_\varphi^{i+1} - \mathbf{H}_\varphi^i}{\Delta r} = \sigma\mathbf{E}_z^i + \varepsilon\dfrac{d}{dt}\mathbf{E}_z^i & \text{on left boundary} \\[5mm] \dfrac{1}{r_i}\mathbf{H}_\varphi^i - \dfrac{\mathbf{H}_\varphi^i - \mathbf{H}_\varphi^{i-1}}{\Delta r} = \sigma\mathbf{E}_z^i + \varepsilon\dfrac{d}{dt}\mathbf{E}_z^i & \text{on right boundary} \end{cases} \tag{5.6}$$

Also like in figure 4.5, left boundary is in wire and right boundary is in air. Finally we get :

$$
\begin{cases}
\mathbf{H}_\varphi^1 - \mathbf{H}_\varphi^0 = \sigma \Delta r \mathbf{E}_z^0 - \Delta r \dfrac{1}{r_0} \mathbf{H}_\varphi^0 & \Rightarrow \quad Sf \\[3mm]
\mathbf{H}_\varphi^{n-1} - \mathbf{H}_\varphi^n = \sigma \Delta r \mathbf{E}_z^n + \varepsilon \Delta r \dfrac{d}{dt} \mathbf{E}_z^n - \Delta r \dfrac{1}{r_n} \mathbf{H}_\varphi^n & \Rightarrow \quad MSf
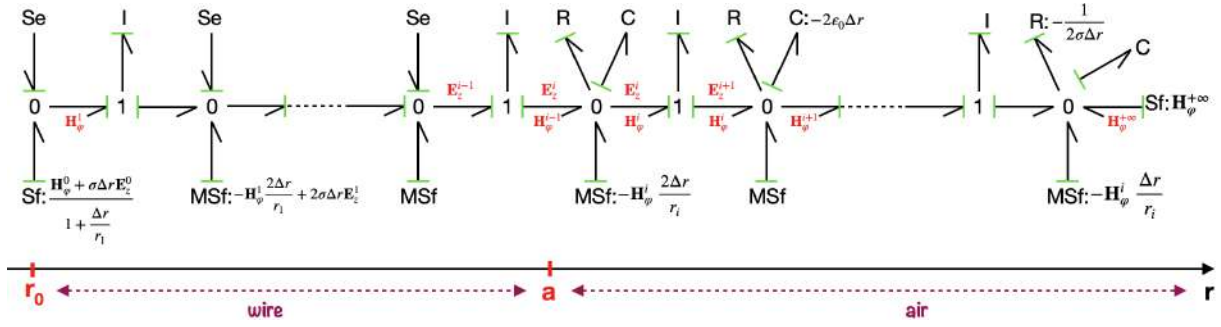\end{cases}
\tag{5.7}
$$

Figure 5.2: Bond graph representation of 1D discrete Maxwell's equations using FVM

5.1.3 Simulation

From the bond graph in figure 5.2, state space equations of the system are derived and aggregated in a system of first order differential equations expresses as equation (4.6). Obviously, state space representation is able to describe variables along time using a numerical integration algorithm such as Euler or Runge-Kutta methods. However, to validate the proposed methodology in magnetostatic condition, we compute static case of the model problem, and then dynamic calculation with state representation.

For the simulation, we use the following discretization of the study domain. $\mathbf{E}$ and $\mathbf{H}$ are calculated in the middle of control volumes.
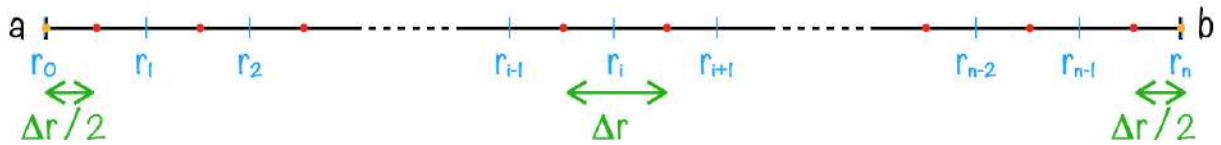

Figure 5.3: Discrete 1D domain

- ├───┤ : control volume
- 🟠 : where we take boundary conditions ($\mathbf{H} = 0$)
- 🔴 : where we compute $\mathbf{E}$ and $\mathbf{H}$
- Infinitely long wire radius : $a = 6\ mm$
- $\Delta r = 0.1\ mm$
- $0 \leqslant r \leqslant 10\ cm$

Static Maxwell's equations give :

$$\begin{cases} \nabla \times \mathbf{E} = 0 \\ \nabla \times \mathbf{H} = \mathbf{J} \end{cases} \tag{5.8}$$

Equation (4.4) becomes :

$$\begin{cases} \dfrac{\partial \mathbf{E}_z}{\partial r} = 0 \\ \dfrac{1}{r}\,\mathbf{H}_\varphi + \dfrac{\partial \mathbf{H}_\varphi}{\partial r} = \sigma \mathbf{E}_z \end{cases} \tag{5.9}$$

Complete FVM methods with interpolation becomes :

$$\sum_i \left(\int_{x_{i-\frac{1}{2}}}^{x_{i+\frac{1}{2}}} \frac{1}{x}\mathbf{H}_\varphi + \frac{\partial \mathbf{H}_\varphi}{\partial x}\,dx = \int_{x_{i-\frac{1}{2}}}^{x_{i+\frac{1}{2}}} \sigma \mathbf{E}_z\,dx \right) \tag{5.10}$$

$$\Rightarrow \quad \sum_i \left(\frac{1}{r_i}\mathbf{H}_\varphi^i + \frac{\mathbf{H}_\varphi^{i+1} - 2\mathbf{H}_\varphi^i + \mathbf{H}_\varphi^{i-1}}{2\Delta r} = \sigma \mathbf{E}_z^i \right) \tag{5.11}$$

$$\Rightarrow \quad \sum_i \frac{1}{r_i}\mathbf{H}_\varphi^i + \frac{1}{2\Delta r} \sum_i \left(\mathbf{H}_\varphi^{i+1} - 2\mathbf{H}_\varphi^i + \mathbf{H}_\varphi^{i-1} \right) = \sum_i \sigma \mathbf{E}_z^i \tag{5.12}$$

On boundary, equation (5.6) becomes

$$\begin{cases} \dfrac{1}{\Delta r}\mathbf{H}_\varphi^1 + \left(\dfrac{1}{r_0} - \dfrac{1}{\Delta r} \right) \mathbf{H}_\varphi^0 = \sigma \mathbf{E}_z^0 & \text{On left boundary} \\ \left(\dfrac{1}{r_n} + \dfrac{1}{\Delta r} \right) \mathbf{H}_\varphi^n - \dfrac{1}{\Delta r}\mathbf{H}_\varphi^{n-1} = \sigma \mathbf{E}_z^n & \text{On right boundary} \end{cases} \tag{5.13}$$

With equation (3.15), the system reduces to :

$$\mathbb{A} \cdot \mathbf{H}_\varphi = \mathbf{J}_\sigma \tag{5.14}$$

- $\mathbf{H}_\varphi = {}^t(\mathbf{H}_\varphi^0,\ \mathbf{H}_\varphi^1,\ \cdots,\ \mathbf{H}_\varphi^n)$

- $\mathbf{J}_\sigma = {}^t(\mathbf{J}_\sigma^0,\ \mathbf{J}_\sigma^1,\ \cdots,\ \mathbf{J}_\sigma^n)$

-

$$\mathbb{A} = \begin{pmatrix} \frac{1}{r_0} - \frac{1}{\Delta r} & \frac{1}{\Delta r} & & & & \\ \frac{1}{2\Delta r} & \left(\frac{1}{r_1} - \frac{1}{\Delta r} \right) & \frac{1}{2\Delta r} & & & \\ & \frac{1}{2\Delta r} & \left(\frac{1}{r_2} - \frac{1}{\Delta r} \right) & \frac{1}{2\Delta r} & & \\ & & \ddots & \ddots & \ddots & \\ & & & \frac{1}{2\Delta r} & \left(\frac{1}{r_{n-1}} - \frac{1}{\Delta r} \right) & \frac{1}{2\Delta r} \\ & & & & \frac{1}{\Delta r} & \frac{1}{r_n} - \frac{1}{\Delta r} \end{pmatrix}$$

Once the static solution has been calculated using the FVM method, we perform the static calculation of the coupled FVM bond graph method using the state representation. The results are compared with those obtained by FDM discretization to validate the scheme.

Based on equation (4.4), and condition $\varepsilon\frac{\partial \mathbf{E}_z}{\partial t} = 0$ in wire, we can deduce that we have 2 states in air and 1 state in wire (corresponding to the system's time derivatives).

$$
\begin{bmatrix} \dot{H}_\varphi \\ \dot{E}_z \end{bmatrix} = \begin{bmatrix} 0 & A_{E_z \to H_\varphi} \\ A_{H_\varphi \to E_z} & A_{E_z} \end{bmatrix} \begin{bmatrix} H_\varphi \\ E_z \end{bmatrix} + \begin{bmatrix} B_{11} & B_{12} & B_{13} \\ B_{21} & B_{22} & B_{23} \\ B_{31} & B_{32} & B_{33} \end{bmatrix} \begin{bmatrix} J_\sigma \\ H_\varphi^0 \\ H_\varphi^{+\infty} \end{bmatrix} \tag{5.15}
$$

In our case we take $\mathbf{H}_\varphi = 0$ on boundaries so, $\mathbf{H}_\varphi^0 = 0$ and $\mathbf{H}_\varphi^{+\infty} = 0$. We get

$$
\begin{bmatrix} \dot{H}_\varphi \\ \dot{E}_z \end{bmatrix} = \begin{bmatrix} 0 & A_{E_z \to H_\varphi} \\ A_{H_\varphi \to E_z} & A_{E_z} \end{bmatrix} \begin{bmatrix} H_\varphi \\ E_z \end{bmatrix} + \begin{bmatrix} B \end{bmatrix} \begin{bmatrix} J_\sigma \end{bmatrix} \tag{5.16}
$$

For the static calculation of the state representation we usually use ${}^t[Hx\ Hy\ Ez] = -(A^{-1}) * B * U$, but in our case the resulting matrices are singular, which leads to an error in code execution.

However, the current taken here is not time-dependent, so the system (5.16) is not time-dependent. An iterative calculation until convergence is therefore used for the simulation.

5.2   FVM scheme in higher dimension [9]

In higher dimensions, we use a Cartesian coordinate system. It's perfectly possible to use the same system for equations in 1-dimensional space, but in our case we wouldn't have been able to apply the simplifying assumptions based on figure 4.2. Using Maxwell's equations in cylindrical coordinates, we were able to verify our FVM modeling and compare the method with that of FDM.

To use FVM approach to solve Maxwell's equations ,

$$
\begin{cases} \nabla \times \mathbf{E} = -\mu\,\dfrac{\partial \mathbf{H}}{\partial t} \\[2mm] \nabla \times \mathbf{H} = \mathbf{J} \end{cases} \tag{5.17}
$$

we need the conservtive form of the system (5.17) to construct the numerical scheme. To get the conservative law we need to rewrite before equation (5.17)

$$
\begin{cases} \nabla \times \mathbf{E} = -\mu\,\dfrac{\partial \mathbf{H}}{\partial t} \\[2mm] \nabla \times \mathbf{H} = \mathbf{J} \end{cases} \quad \Rightarrow \quad \begin{cases} \nabla \times \mathbf{E} = -\mu\,\dfrac{\partial \mathbf{H}}{\partial t} \\[2mm] \nabla \times \mathbf{H} = \mathbf{J}_s + \sigma\mathbf{E} + \varepsilon\,\dfrac{\partial \mathbf{E}}{\partial t} \end{cases}
$$

$\mathbf{J}_s = 0$, so we get :

$$\begin{cases} \mu \, \dfrac{\partial \mathbf{H}}{\partial t} & = -\nabla \times \mathbf{E} \\[2mm] \varepsilon \, \dfrac{\partial \mathbf{E}}{\partial t} & = \nabla \times \mathbf{H} \, - \, \mathbf{J}_\sigma \end{cases} \tag{5.18}$$

The conservative form of system (5.18) is given by :

$$\alpha \, \frac{\partial \mathbf{Q}}{\partial t} \, + \, \nabla \cdot \mathbb{F}(\mathbf{Q}) \, = \, -\mathbf{J} \tag{5.19}$$

where $\quad \alpha = (\mu, \, \varepsilon) \quad , \quad \mathbf{Q} = {}^t(\mathbf{E}, \, \mathbf{H}) \quad , \quad \mathbf{J} = {}^t(0, \, \mathbf{J}_\sigma) \quad$ and $\quad \mathbb{F}$ described a curl operator in dimension d for ${}^t(\mathbf{H}, \, \mathbf{E})$.

Consider the elements of the mesh as control volumes and integrate the conservative form (5.19) over each control volume $\mathbf{V}$:

$$\int_{\mathbf{V}} \left(\alpha \, \frac{\partial \mathbf{Q}}{\partial t} \, + \, \nabla \cdot \mathbb{F}(\mathbf{Q}) \right) dv \, = \, - \int_{\mathbf{V}} \mathbf{J} \, dv \tag{5.20}$$

Applying Green - Ostrogradsky's theorem gives :

$$\int_{\mathbf{V}} \alpha \, \frac{\partial \mathbf{Q}}{\partial t} \, dv \, + \, \int_{\partial \mathbf{V}} \mathbb{F}(\mathbf{Q}) \cdot \mathbf{n} \, ds \, = \, - \int_{\mathbf{V}} \mathbf{J} \, dv \tag{5.21}$$

which implies

$$\int_{\mathbf{V}} \alpha \, \frac{\partial \mathbf{Q}}{\partial t} \, dv \, + \, \sum_{\mathbf{V}' \in \mathbf{P}(\mathbf{V})} \int_{\partial \mathbf{V} \cap \partial \mathbf{V}'} \mathbb{F}(\mathbf{Q}) \cdot \mathbf{n} \, ds \, = \, - \int_{\mathbf{V}} \mathbf{J} \, dv \tag{5.22}$$

where $\mathbf{n}$ is the outward unit vector normal to $\mathbf{V}$ and $\mathbf{P}(\mathbf{V})$ denotes the set of neighbours of the volume $\mathbf{V}$.

Let $\hat{\mathbb{F}}(\mathbf{Q})$ an approximation of $\mathbb{F}(\mathbf{Q})$ at the interface $\partial \mathbf{V} \cap \partial \mathbf{V}'$ and

$$\eta = \int_{\partial \mathbf{V} \cap \partial \mathbf{V}'} \mathbf{n} \, ds. \tag{5.23}$$

We denote the flux exchanged between the volume and its neighbours by the following function

$$\mathbf{\Phi}(\mathbf{Q_V}, \, \mathbf{Q_{V'}}) \, = \, \hat{\mathbb{F}}(\mathbf{Q}) \cdot \eta \tag{5.24}$$

where $\mathbf{Q_V}$ is the value of the field on the volume $\mathbf{V}$.

Suppose that the time derivative is constant on each volume $\mathbf{V}$, then we obtain the following formulation :

$$Volume(\mathbf{V}) \, \left(\alpha \, \frac{\partial \mathbf{Q}}{\partial t} \right) \, + \, \sum_{\mathbf{V}' \in \mathbf{P}(\mathbf{V})} \mathbf{\Phi}(\mathbf{Q_V}, \, \mathbf{Q_{V'}}) \, = \, 0. \tag{5.25}$$

To evaluate the function $\boldsymbol{\Phi}$, we choose the centered flux defined by :

$$\boldsymbol{\Phi}(U,\,U') \;=\; \frac{\mathcal{F}(U,\,\eta) \;+\; \mathcal{F}(U',\,\eta)}{2} \tag{5.26}$$

with

- $\mathcal{F}(U,\,\eta) \;=\; \eta \cdot \mathbb{F}(U)$

- $\boldsymbol{\Phi} \;=\; {}^{t}(\boldsymbol{\Phi_E},\,\boldsymbol{\Phi_H})$

After a space discretization, we obtain the following ODE :

$$\begin{cases} \mu\,\dfrac{d\mathbf{H}}{dt} \;+\; \Psi_1(\mathbf{E}) \;=\; 0 \\[2mm] \varepsilon\,\dfrac{d\mathbf{E}}{dt} \;+\; \Psi_2(\mathbf{H}) \;=\; -\sigma\mathbf{E} \end{cases} \tag{5.27}$$

Stability and convergence of this method have been established for Cartesian meshes in [9] and for unstructured meshes in [8].

5.2.1   Representation in 2D case

Since the curl is a 3-dimensional operator, let's start by reminding how to write system (5.18) in 3 dimensions in Cartesian coordinates.

$$\begin{cases} \mu\,\dfrac{\partial \mathbf{H}_x}{\partial t} \;+\; \left(\dfrac{\partial \mathbf{E}_z}{\partial y} - \dfrac{\partial \mathbf{E}_y}{\partial z}\right) \;=\; 0 & (1) \\[3mm] \mu\,\dfrac{\partial \mathbf{H}_y}{\partial t} \;+\; \left(\dfrac{\partial \mathbf{E}_x}{\partial z} - \dfrac{\partial \mathbf{E}_z}{\partial x}\right) \;=\; 0 & (2) \\[3mm] \mu\,\dfrac{\partial \mathbf{H}_z}{\partial t} \;+\; \left(\dfrac{\partial \mathbf{E}_y}{\partial x} - \dfrac{\partial \mathbf{E}_x}{\partial y}\right) \;=\; 0 & (3) \\[3mm] \varepsilon\,\dfrac{\partial \mathbf{E}_x}{\partial t} \;-\; \left(\dfrac{\partial \mathbf{H}_z}{\partial y} - \dfrac{\partial \mathbf{H}_y}{\partial z}\right) \;=\; -\mathbf{J}_{\sigma_x} & (4) \\[3mm] \varepsilon\,\dfrac{\partial \mathbf{E}_y}{\partial t} \;-\; \left(\dfrac{\partial \mathbf{H}_x}{\partial z} - \dfrac{\partial \mathbf{H}_z}{\partial x}\right) \;=\; -\mathbf{J}_{\sigma_y} & (5) \\[3mm] \varepsilon\,\dfrac{\partial \mathbf{E}_z}{\partial t} \;-\; \left(\dfrac{\partial \mathbf{H}_y}{\partial x} - \dfrac{\partial \mathbf{H}_x}{\partial y}\right) \;=\; -\mathbf{J}_{\sigma_z} & (6) \end{cases} \tag{5.28}$$

[5]In two-dimensional space for the Cartesian coordinate system, we just have x and y. So one needs to simplify the system to take account this condition. We can see from equations (3) and (6) of system (5.28) that it is possible to define $\mathbf{E}$ or $\mathbf{H}$ in the plane transverse to the study plane with respect to $\mathbf{H}$ and $\mathbf{E}$ respectively in the study plane.

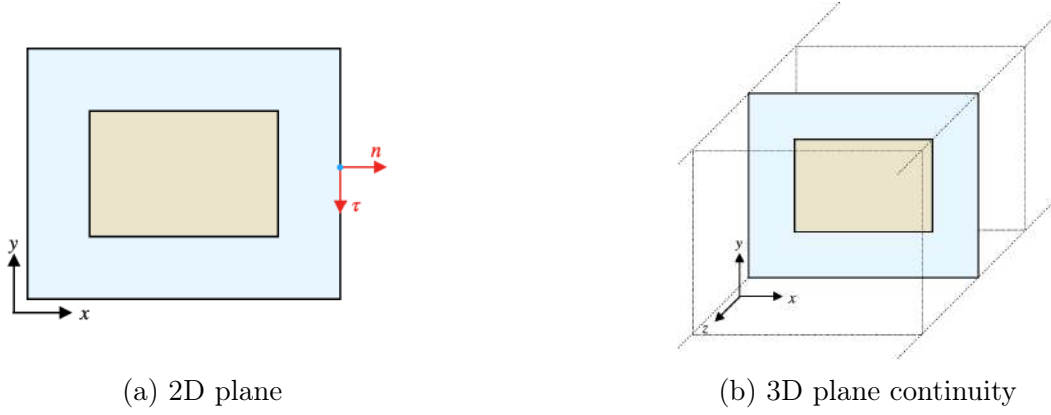(a) 2D plane   (b) 3D plane continuity

Figure 5.4: Transverse plane representation

Equation (5.28) can be equivalent written as two decouples systems for $(\mathbf{H}_\perp, \mathbf{E}_z)$ and $(\mathbf{E}_\perp, \mathbf{H}_z)$, where we have to introduced the transverse fields $\mathbf{E}_\perp := {}^t(\mathbf{E}_x, \mathbf{E}_y)$ and $\mathbf{H}_\perp := {}^t(\mathbf{H}_x, \mathbf{H}_y)$. We also introduce, for the sake of conciseness, the following 2D differential operators :

$$u \mapsto \mathbf{curl}\, u = \boldsymbol{\nabla} \times u = {}^t\left(\frac{\partial u}{\partial y}, \frac{\partial u}{\partial x}\right) \tag{5.29}$$

$$\mathbf{u} = {}^t(u_x, u_y) \mapsto curl(\mathbf{u}) = \nabla \times \mathbf{u} = \frac{\partial u_y}{\partial x} - \frac{\partial u_x}{\partial y} \tag{5.30}$$

The first problem involves the unknowns $(\mathbf{H}_\perp, \mathbf{E}_z)$ and is called the TE problem (where TE stands for Transverse Electric). The second one involves the unknowns $(\mathbf{E}_\perp, \mathbf{H}_z)$ and is called the TM problem (where TM stands for Transverse Magnetic).

For the purposes of this internship, we have chosen the TE problem formulation. This is logical, firstly because we want to calculate the static magnetic field in order to apply the state-space representation later, and secondly it will enable us to verify the right-hand rule (figure 4.2).

$$\begin{cases} \mu\, \dfrac{\partial \mathbf{H}_x}{\partial t} + \dfrac{\partial \mathbf{E}_z}{\partial y} = 0 & (1) \\[2mm] \mu\, \dfrac{\partial \mathbf{H}_y}{\partial t} - \dfrac{\partial \mathbf{E}_z}{\partial x} = 0 & (2) \\[2mm] \varepsilon\, \dfrac{\partial \mathbf{E}_z}{\partial t} - \left(\dfrac{\partial \mathbf{H}_y}{\partial x} - \dfrac{\partial \mathbf{H}_x}{\partial y}\right) = -\mathbf{J}_{\sigma_z} & (3) \end{cases} \tag{5.31}$$

From equation (5.31) we can therefore write the following conservation law [3] :

$$\alpha\, \frac{\partial \mathbf{Q}}{\partial t} + \nabla \cdot \mathbb{F}(\mathbf{Q}) = -\mathbf{J} \tag{5.32}$$

$$\alpha = {}^t(\mu, \mu, \varepsilon), \qquad \mathbf{Q} = {}^t(\mathbf{H}_\perp, \mathbf{E}_z), \qquad \mathbb{F} = (\mathbf{F}_1, \mathbf{F}_2)$$

$$\mathbf{F}_1(\mathbf{Q}) = {}^t(0, -\mathbf{E}_z, -\mathbf{H}_y), \quad \mathbf{F}_2(\mathbf{Q}) = {}^t(\mathbf{E}_z, 0, \mathbf{H}_x), \quad \mathbf{J} = {}^t(0, 0, \mathbf{J}_{\sigma_z})$$

then we obtain the following space discretization :

$$\begin{cases} \mu \dfrac{d\mathbf{H}}{dt} + \dfrac{1}{aire(\mathbf{V}_i)} \displaystyle\sum_{\mathbf{E}_j \in \mathbf{P}(\mathbf{E}_i)} \dfrac{\eta}{2}(\mathbb{F}(\mathbf{E}_i) + \mathbb{F}(\mathbf{E}_j)) = 0 \qquad (1) \\[4mm] \varepsilon \dfrac{d\mathbf{E}}{dt} + \dfrac{1}{aire(\mathbf{V}_i)} \displaystyle\sum_{\mathbf{H}_j \in \mathbf{P}(\mathbf{H}_i)} \dfrac{\eta}{2}(\mathbb{F}(\mathbf{H}_i) + \mathbb{F}(\mathbf{H}_j)) = -\sigma\mathbf{E} \qquad (2) \end{cases} \qquad (5.33)$$

$$\mathbf{E} = \mathbf{E}_z \quad , \quad \mathbf{H} = \left\{ \begin{array}{c} \mathbf{H}_x \\ \mathbf{H}_y \end{array} \right\} \quad , \quad \mathbb{F}(\mathbf{H}) = \mathbf{H}_y - \mathbf{H}_x \quad , \quad \mathbb{F}(\mathbf{E}) = \left\{ \begin{array}{c} -\mathbf{E}_z \\ \mathbf{E}_z \end{array} \right\}.$$

From this we can write our bond graph model :

➤ Faraday's law $\Rightarrow$ $\quad \mathbf{H} = \dfrac{1}{\mu \, aire(\mathbf{V}_i)} \displaystyle\sum_{\mathbf{E}_j \in \mathbf{P}(\mathbf{E}_i)} \dfrac{\eta}{2} \int_t (\mathbb{F}(\mathbf{E}_i) + \mathbb{F}(\mathbf{E}_j)) \, d\tau$

$\quad \Rightarrow \quad$ multiport I and 1-junction

➤ Ampere's law $\Rightarrow$ $\quad \displaystyle\sum_{\mathbf{H}_j \in \mathbf{P}(\mathbf{H}_i)} \eta \, (\mathbb{F}(\mathbf{H}_i) + \mathbb{F}(\mathbf{H}_j)) = -2\sigma \, aire(\mathbf{V}_i) \, \mathbf{E} - 2\varepsilon \, aire(\mathbf{V}_i) \dfrac{d\mathbf{E}}{dt}$

$\quad \Rightarrow \quad$ 0-junction

➥ In wire $\quad \varepsilon \dfrac{d\mathbf{E}}{dt} = \varepsilon \dfrac{\partial \mathbf{E}_z}{\partial t} = 0 \Rightarrow \quad$ multiport R

➥ In air $\quad \varepsilon \dfrac{d\mathbf{E}}{dt} = \varepsilon \dfrac{\partial \mathbf{E}_z}{\partial t} \neq 0 \Rightarrow \quad$ multiport R, multiport C

➥ On boundary, $\mathbb{F}(\mathbf{H}_i) = -\dfrac{2\sigma \, aire(\mathbf{V}_i)}{\zeta} \mathbf{E} - \dfrac{2\varepsilon \, aire(\mathbf{V}_i)}{\zeta} \dfrac{d\mathbf{E}}{dt} - \dfrac{\displaystyle\sum_{\mathbf{H}_j \in \mathbf{P}(\mathbf{H}_i)} \eta\mathbb{F}(\mathbf{H}_j)}{\zeta}$

$\quad \zeta = \displaystyle\sum_{\mathbf{H}_j \in \mathbf{P}(\mathbf{H}_i)} \eta + 2 \sum_{\partial\mathbf{H}_i \in \partial\Omega} \eta$

$\quad \Rightarrow \quad$ multiport R, multiport C, multiport Sf

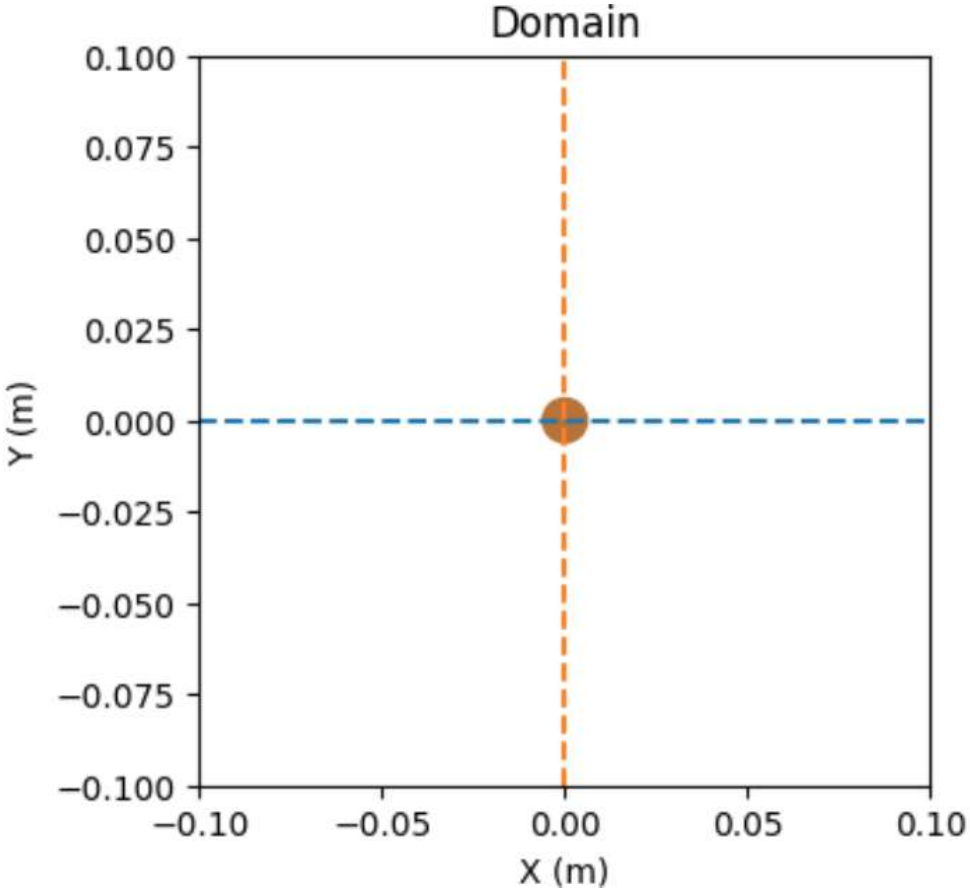For the 2D model of our test case (figure 5.5)we get :
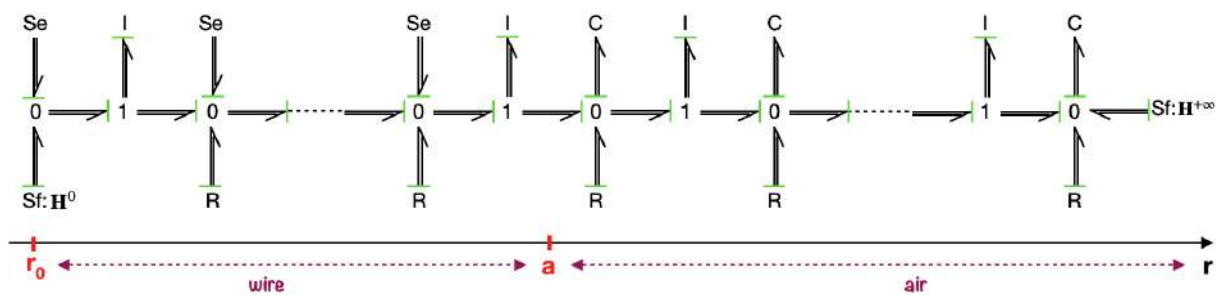
Figure 5.5: 2D domain

Figure 5.6: 2D model Bond Graph

To better understand the structure of the bond graph at the scale of a cell and its neighborhood, we can use a semi-bond graph model centered on this element.
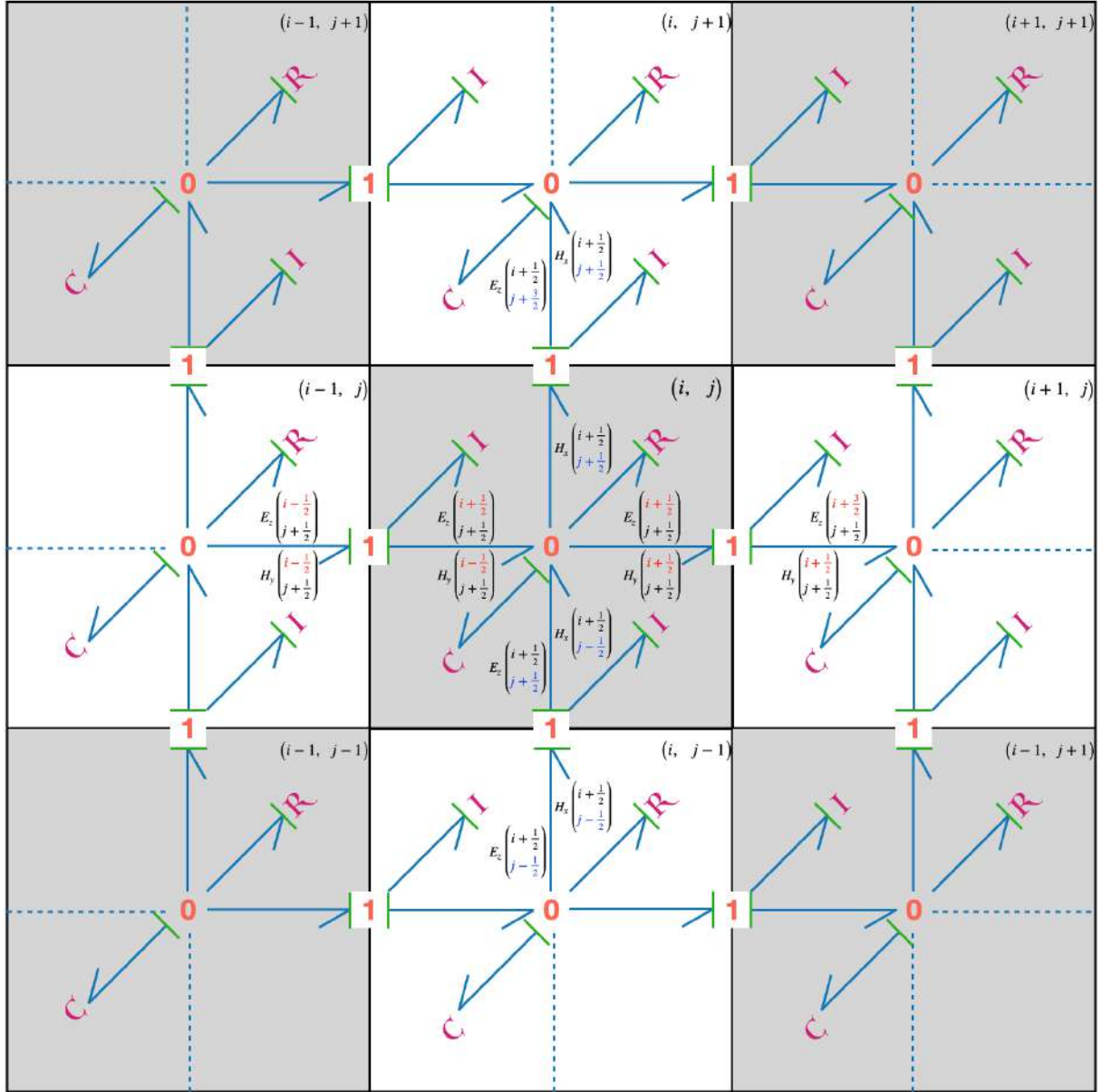
Figure 5.7: 2D semi Bond Graph of a cell with neighborhood in air only

Simulation

For ease of understanding, let's consider a Cartesian structured mesh with a fixed pitch. In the case of an unstructured mesh, Δx and Δy are replaced by a step h_i. Like in 1D case, we simulate FVM method and state representation statically. From the equations (3) in (5.31) and (2) in (5.33)

$$\frac{1}{2\Delta x}\{\mathbf{H}_y^{i+\frac{3}{2},\,j+\frac{1}{2}} - \mathbf{H}_y^{i-\frac{1}{2},\,j+\frac{1}{2}}\} - \frac{1}{2\Delta y}\{\mathbf{H}_x^{i+\frac{1}{2},\,j+\frac{3}{2}} - \mathbf{H}_x^{i+\frac{1}{2},\,j-\frac{1}{2}}\} = \mathbf{J}_{\sigma_z}^{i+\frac{1}{2},\,j+\frac{1}{2}}$$

The complete finite volume scheme reduces to

$$A_y \cdot \mathbf{H}_y - A_x \cdot \mathbf{H}_x = \mathbf{J}_{\sigma_z} \qquad \Rightarrow \qquad (A_y \mid -A_x) \cdot \begin{pmatrix} \mathbf{H}_y \\ \mathbf{H}_x \end{pmatrix} = \mathbf{J}_{\sigma_z}. \qquad (5.34)$$

The system is solved using an SVD method (Singular Value Decomposition).

To get an idea of the structure of the resulting matrices, let's take an example of the discretization of a domain into 4×4.
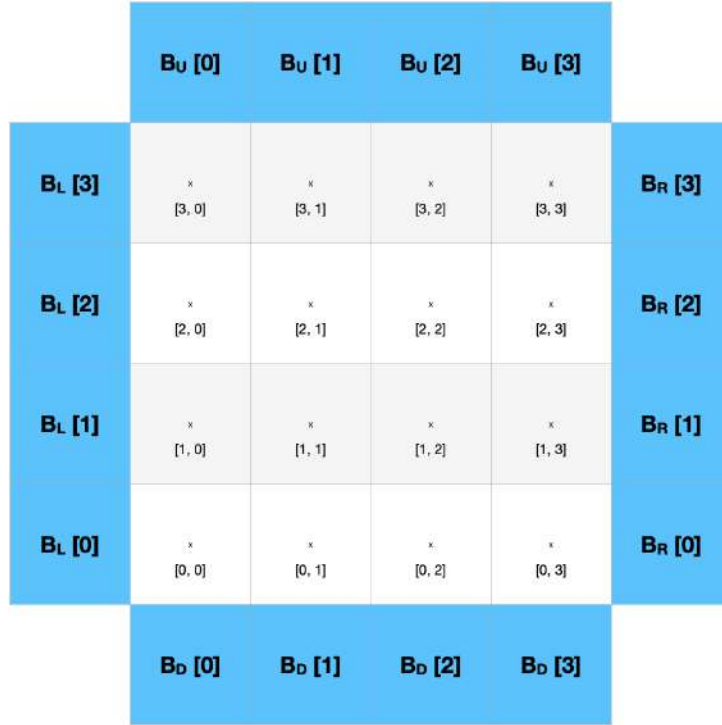

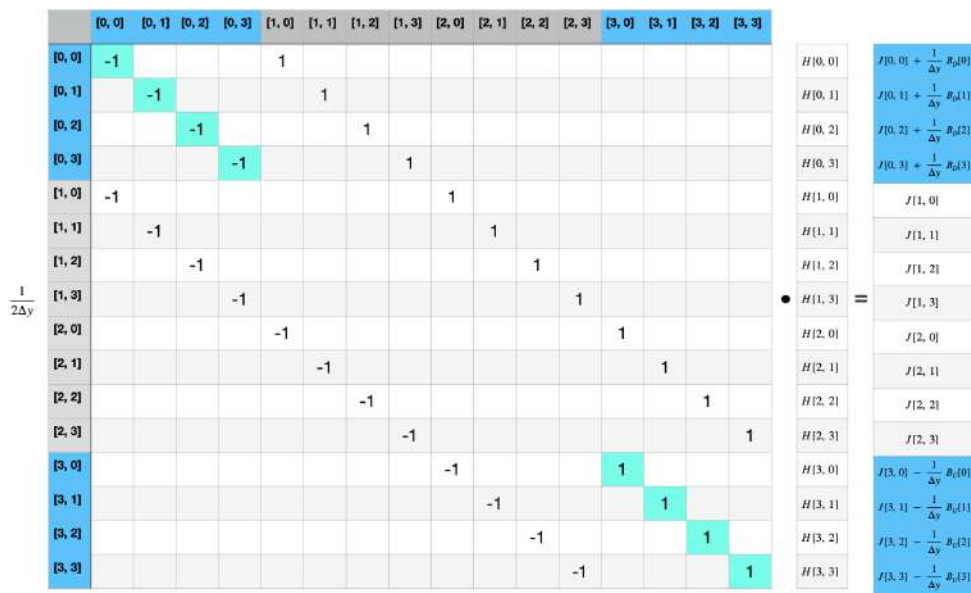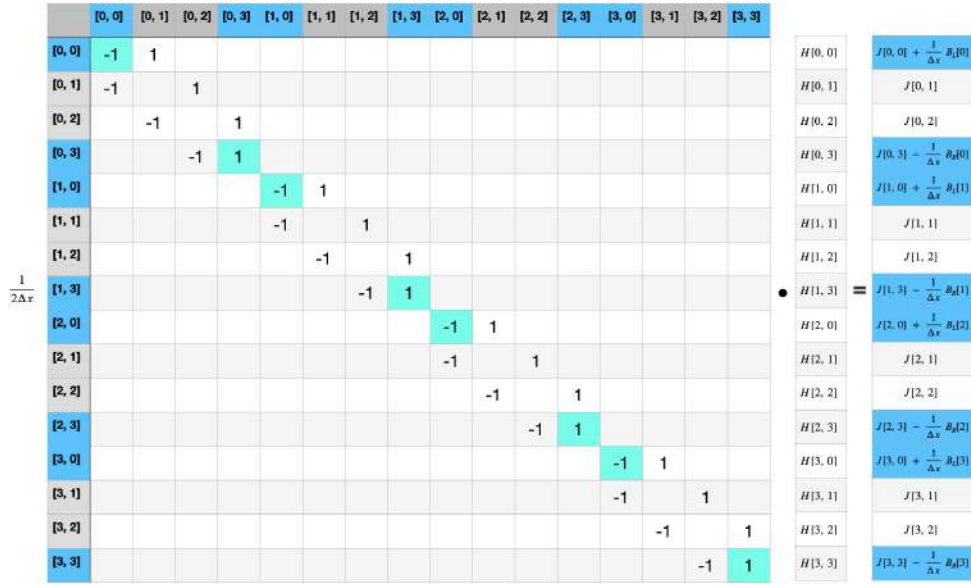Figure 5.8: Discret domain with boundary conditions
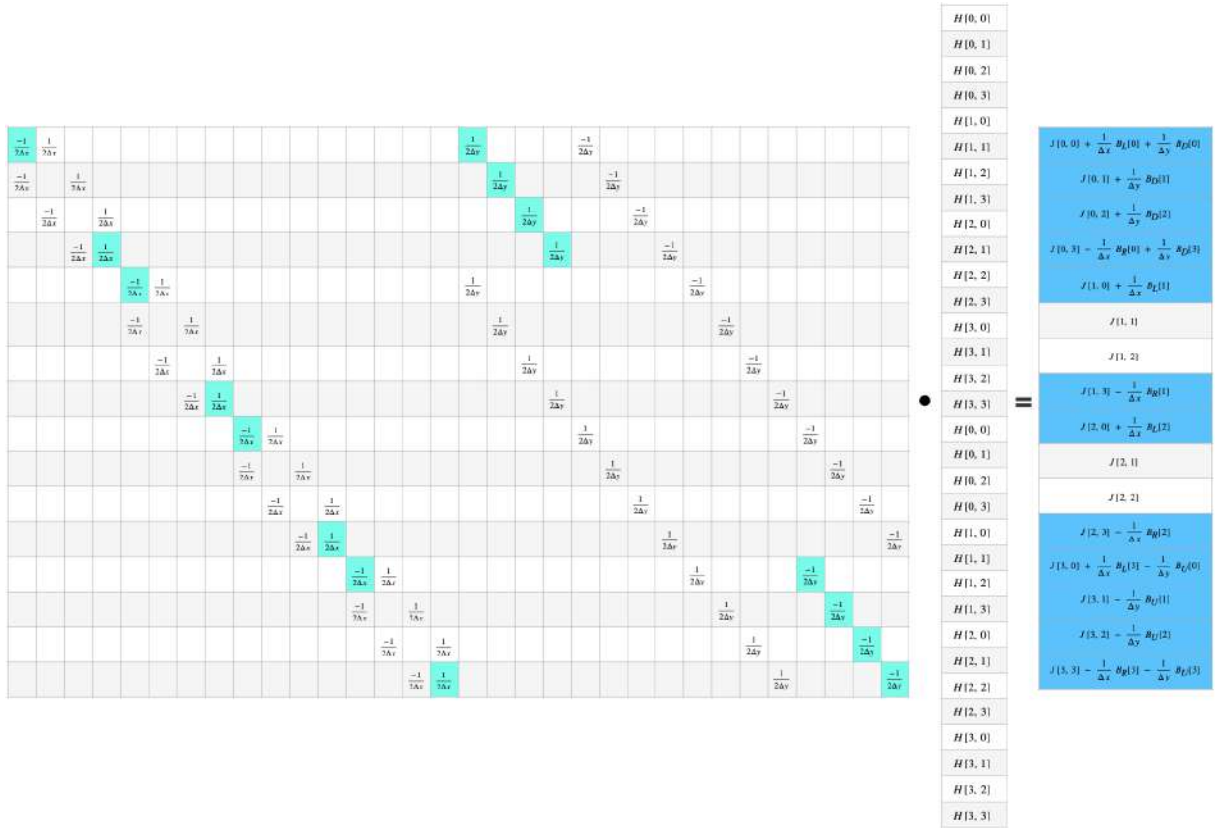

Figure 5.9: Ax

Figure 5.10: Ay

Figure 5.11: Global matrix assemble

Based on equation (5.31), and condition $\varepsilon \dfrac{d\mathbf{E}}{dt} = 0$ in wire, we can deduce that we have 3 states in air and 2 states in wire (corresponding to the system's time derivatives). In

our case we take $\mathbf{H}_\perp = 0$ on boundary, so we get :

$$\begin{bmatrix} \dot{H}_x \\ \dot{H}_y \\ \dot{E}_z \end{bmatrix} = \begin{bmatrix} 0 & 0 & A_{E_z \to H_x} \\ 0 & 0 & A_{E_z \to H_y} \\ A_{H_x \to E_z} & A_{H_y \to E_z} & A_{E_z} \end{bmatrix} \begin{bmatrix} H_x \\ H_y \\ E_z \end{bmatrix} + \begin{bmatrix} B \end{bmatrix} \begin{bmatrix} J_\sigma \end{bmatrix} \tag{5.35}$$

The sub-blocks of matrix A in this state representation have the same structure as those presented above (A_x, and A_y), except for A_{E_z}, which is a diagonal matrix.

5.2.2 Representation in 3D case

Based on equation (5.28), we get the following conservation law [9]:

$$\alpha \frac{\partial \mathbf{Q}}{\partial t} + \nabla \cdot \mathbb{F}(\mathbf{Q}) = -\mathbf{J}_\sigma \tag{5.36}$$

$$\alpha \;=\; {}^t(\mu, \varepsilon) \quad , \quad \mathbf{Q} \;=\; {}^t(\mathbf{H}, \mathbf{E}) \quad , \quad \mathbb{F} \;=\; (\mathbf{F}_1, \mathbf{F}_2, \mathbf{F}_3)$$

$$\mathbf{F}_1(\mathbf{Q}) = \begin{Bmatrix} 0 \\ -\mathbf{E}_z \\ \mathbf{E}_y \\ 0 \\ \mathbf{H}_z \\ -\mathbf{H}_y \end{Bmatrix}, \; \mathbf{F}_2(\mathbf{Q}) = \begin{Bmatrix} \mathbf{E}_z \\ 0 \\ -\mathbf{E}_x \\ -\mathbf{H}_z \\ 0 \\ \mathbf{H}_x \end{Bmatrix}, \; \mathbf{F}_3(\mathbf{Q}) = \begin{Bmatrix} -\mathbf{E}_y \\ \mathbf{E}_x \\ 0 \\ \mathbf{H}_y \\ -\mathbf{H}_x \\ 0 \end{Bmatrix}, \; \mathbf{J}_f = \begin{Bmatrix} 0 \\ 0 \\ 0 \\ \mathbf{J}_{\sigma_x} \\ \mathbf{J}_{\sigma_y} \\ \mathbf{J}_{\sigma_z} \end{Bmatrix}.$$

Then we can write the space discretization

$$\begin{cases} \mu \, \dfrac{d\mathbf{H}}{dt} \;+\; \dfrac{1}{volume(\mathbf{V})} \displaystyle\sum_{\mathbf{E}' \in \mathbf{P}(\mathbf{E})} \dfrac{\eta}{2}(\mathbb{F}(\mathbf{E}) + \mathbb{F}(\mathbf{E}')) \;=\; 0 \qquad (1) \\[4mm] \varepsilon \, \dfrac{d\mathbf{E}}{dt} \;+\; \dfrac{1}{volume(\mathbf{V})} \displaystyle\sum_{\mathbf{H}' \in \mathbf{P}(\mathbf{H})} \dfrac{\eta}{2}(\mathbb{F}(\mathbf{H}) + \mathbb{F}(\mathbf{H}')) \;=\; -\mathbf{J}_\sigma \qquad (2) \end{cases} \tag{5.37}$$

From this discretization, we can write our bond graph model :

➢ Faraday's law $\Rightarrow$ $\mathbf{H} = \dfrac{1}{\mu \; volume(\mathbf{V})} \displaystyle\sum_{\mathbf{E}' \in \mathbf{P}(\mathbf{E})} \dfrac{\eta}{2} \int_t (\mathbb{F}(\mathbf{E}) + \mathbb{F}(\mathbf{E}')) \; d\tau$

$\Rightarrow$ multiport I and 1-junction

➢ Ampere's law $\Rightarrow$ $\displaystyle\sum_{\mathbf{H}' \in \mathbf{P}(\mathbf{H})} \eta \, (\mathbb{F}(\mathbf{H}) + \mathbb{F}(\mathbf{H}')) = -2\sigma \, volume(\mathbf{V}) \, \mathbf{E} - 2\varepsilon \, volume(\mathbf{V}) \dfrac{d\mathbf{E}}{dt}$

$\Rightarrow$ 0-junction

➥ In wire $\varepsilon \dfrac{d\mathbf{E}}{dt} = 0 \Rightarrow$ multiport R

➥ In air $\varepsilon \dfrac{d\mathbf{E}}{dt} \neq 0 \Rightarrow$ multiport R, multiport C

➥ On boundary, $\mathbb{F}(\mathbf{H}) = -\dfrac{2\sigma \; volume(\mathbf{V})}{\zeta} \mathbf{E} - \dfrac{2\varepsilon \; volume(\mathbf{V})}{\zeta} \dfrac{d\mathbf{E}}{dt} - \dfrac{\displaystyle\sum_{\mathbf{H}' \in \mathbf{P}(\mathbf{H})} \eta \mathbb{F}(\mathbf{H}')}{\zeta}$

$\zeta = \displaystyle\sum_{\mathbf{H}' \in \mathbf{P}(\mathbf{H})} \eta + 2 \sum_{\partial\mathbf{H} \in \partial\Omega} \eta$

$\Rightarrow$ multiport R, multiport C, multiport Sf

We obtain the same bond graph as in 2D model (figure 5.6).

FVM Simulation

For ease of understanding, let's consider a Cartesian structured mesh with a fixed pitch. In the case of an unstructured mesh, Δx, Δy and Δz are replaced by a step h_i. From equations (4), (5), (6) in (5.28) and (2) in (5.37). (Here i, j, k stand for $i+\frac{1}{2}$, $j+\frac{1}{2}$, $k+\frac{1}{2}$)

$$
\begin{cases}
\dfrac{1}{2\Delta y} \{\mathbf{H}_z^{i,\,j+1,\,k} - \mathbf{H}_z^{i,\,j-1,\,k}\} - \dfrac{1}{2\Delta z} \{\mathbf{H}_y^{i,\,j,\,k+1} - \mathbf{H}_y^{i,\,j,\,k-1}\} = \mathbf{J}_{\sigma_x}^{i,\,j,\,k} \\[2ex]
\dfrac{1}{2\Delta z} \{\mathbf{H}_x^{i,\,j,\,k+1} - \mathbf{H}_x^{i,\,j,\,k-1}\} - \dfrac{1}{2\Delta x} \{\mathbf{H}_z^{i+1,\,j,\,k} - \mathbf{H}_z^{i-1,\,j,\,k}\} = \mathbf{J}_{\sigma_y}^{i,\,j,\,k} \\[2ex]
\dfrac{1}{2\Delta x} \{\mathbf{H}_y^{i+1,\,j\,k} - \mathbf{H}_y^{i-1,\,j,\,k}\} - \dfrac{1}{2\Delta y} \{\mathbf{H}_x^{i,\,j+1,\,k} - \mathbf{H}_x^{i,\,j-1,\,k}\} = \mathbf{J}_{\sigma_z}^{i,\,j,\,k}
\end{cases}
$$

The complete finite volume scheme reduces to

$$
\begin{cases}
A_z \cdot \mathbf{H}_z - A_y \cdot \mathbf{H}_y = \mathbf{J}_{\sigma_x} \\
A_x \cdot \mathbf{H}_x - A_z \cdot \mathbf{H}_z = \mathbf{J}_{\sigma_y} \\
A_y \cdot \mathbf{H}_y - A_x \cdot \mathbf{H}_x = \mathbf{J}_{\sigma_z}
\end{cases}
\Rightarrow
\begin{bmatrix} 0 & -A_y & A_z \\ A_x & 0 & -A_z \\ -A_x & A_y & 0 \end{bmatrix}
\begin{bmatrix} \mathbf{H}_x \\ \mathbf{H}_y \\ \mathbf{H}_z \end{bmatrix}
=
\begin{bmatrix} \mathbf{J}_x \\ \mathbf{J}_y \\ \mathbf{J}_z \end{bmatrix}
\quad (5.38)
$$

State representation

Based on equation (5.28), and condition $\varepsilon \dfrac{d\mathbf{E}}{dt} = 0$ in wire, we can deduce that we have 6 states in air and 3 states in wire (corresponding to the system's time derivatives).

Suppose $\mathbf{H} = 0$ on boundary, so we get :

$$
\begin{bmatrix} \dot{H}_x \\ \dot{H}_y \\ \dot{H}_z \\ \dot{E}_x \\ \dot{E}_y \\ \dot{E}_z \end{bmatrix} = \begin{bmatrix} 0 & 0 & 0 & 0 & A_{E_y \to H_x} & A_{E_z \to H_x} \\ 0 & 0 & 0 & A_{E_x \to H_y} & 0 & A_{E_x \to H_y} \\ 0 & 0 & 0 & A_{E_x \to H_z} & A_{E_y \to H_z} & 0 \\ 0 & A_{H_y \to E_x} & A_{H_z \to E_x} & A_{E_x} & 0 & 0 \\ A_{H_x \to E_y} & 0 & A_{H_z \to E_y} & 0 & A_{E_y} & 0 \\ A_{H_x \to E_z} & A_{H_y \to E_z} & 0 & 0 & 0 & A_{E_z} \end{bmatrix} \begin{bmatrix} H_x \\ H_y \\ H_z \\ E_x \\ E_y \\ E_z \end{bmatrix} + \begin{bmatrix} B \end{bmatrix} \begin{bmatrix} J_\sigma \end{bmatrix}
$$

$$(5.39)$$

6. Results

Here, we will only present the magnetic field results obtained after calculating statical Maxwell's equations in two dimensions of space (Ampere's law and Faraday's law) using FVM. This is due to the fact that we currently have a singularity problem (being solved) in the A matrix of the state space representation.

- Infinitely long wire radius : $a = 6\ mm$
- $\Delta x = \Delta y = 0.2\ mm$
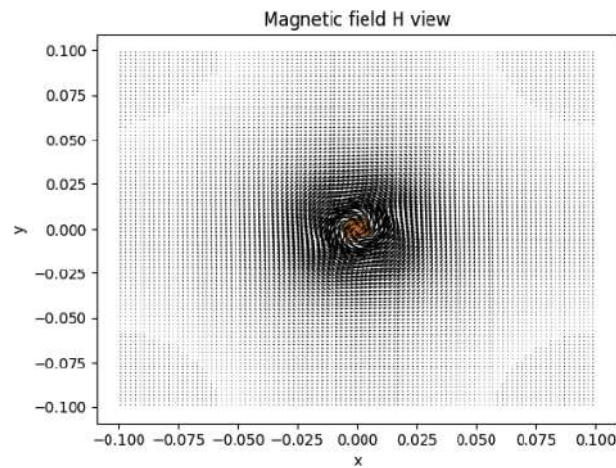- $0 \leqslant x, y \leqslant 10\ cm$
- $I = 20\ A$

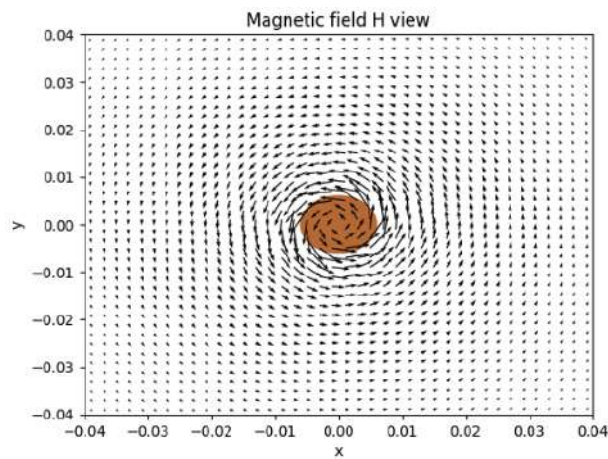Figure 6.1: Circulation of magnetic field

Figure 6.2: Circulation of magnetic field zoomed on wire

Figure 6.2 shows that our magnetic field simulation using FVM respects the Ampère's right-hand grip rule 4.2.

To visualize the magnetic field, we can also use its magnitude :

$$|\mathbf{H}| \quad = \quad \sqrt{\mathbf{H}_x^2 \; + \; (\mathbf{H}_y^2} \tag{6.1}$$

Magnetic field magnitude is the strength of the magnetic field at a given point, regardless of direction. It represents the absolute value of the magnetic field intensity. It therefore indicates how strong or weak the magnetic field is. This is useful in the design of electronic and electromagnetic equipment such as transformers, where the strength of the magnetic field influences performance and efficiency.
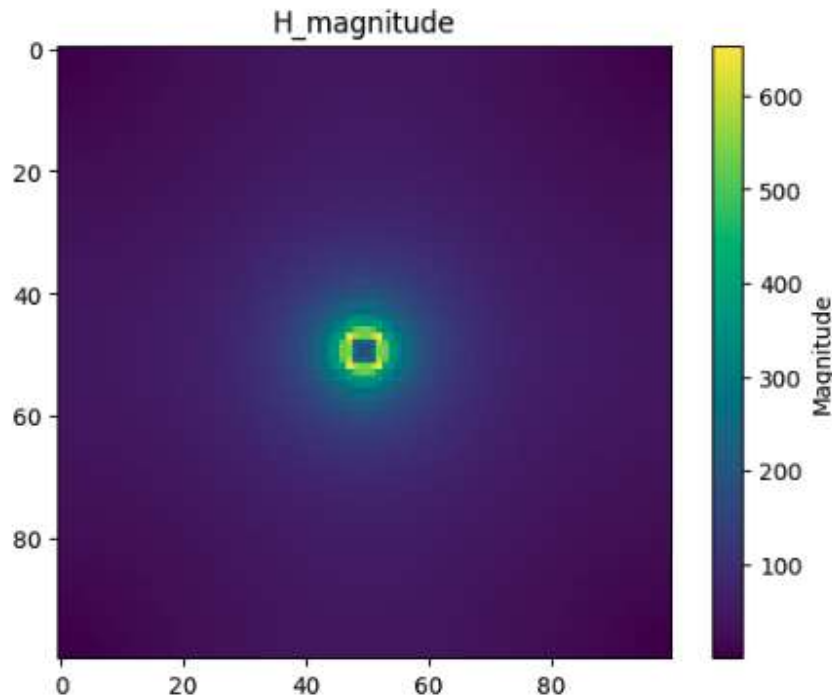

Figure 6.3: Magnitude

To validate the results, we compared them with those of the 1D model. In theory, when we calculate $\mathbf{H}_{\mathbf{x}}$ as a function of x and $\mathbf{H}_{\mathbf{y}}$ as a function of y, we should have the same curve as that obtained with $\mathbf{H}_{\varphi}$ in 1D (with the exception of the sign). $\mathbf{H}_{\mathbf{x}}$ as a function of y and $\mathbf{H}_{\mathbf{y}}$ as a function of x must be uniformly equal to 0.
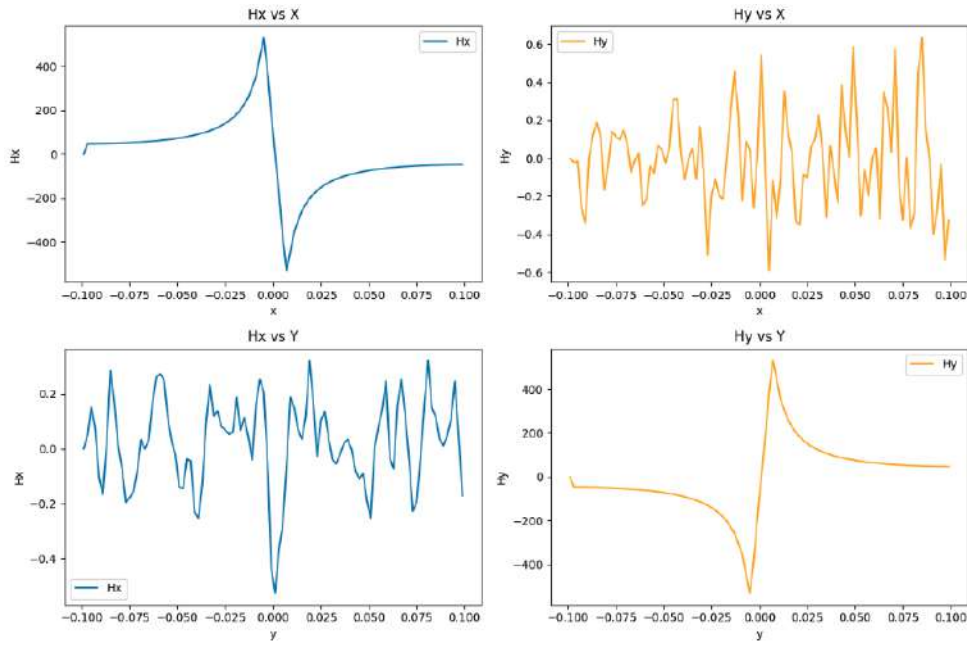
Figure 6.4: Comparison with the analytical solution

To validate the model, we calculate the diagonal and antidiagonal of $\mathbf{H_x}$ and $\mathbf{H_y}$. For the anti-diagonal, we need to have the same 4 curves as above, and for the diagonal, we need to have symmetry along the x-axis.
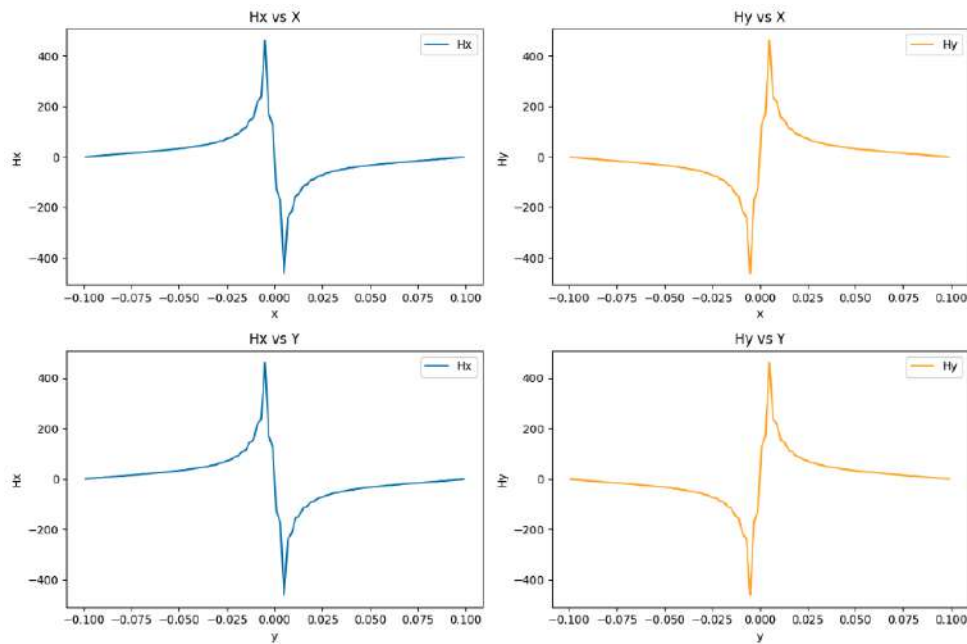

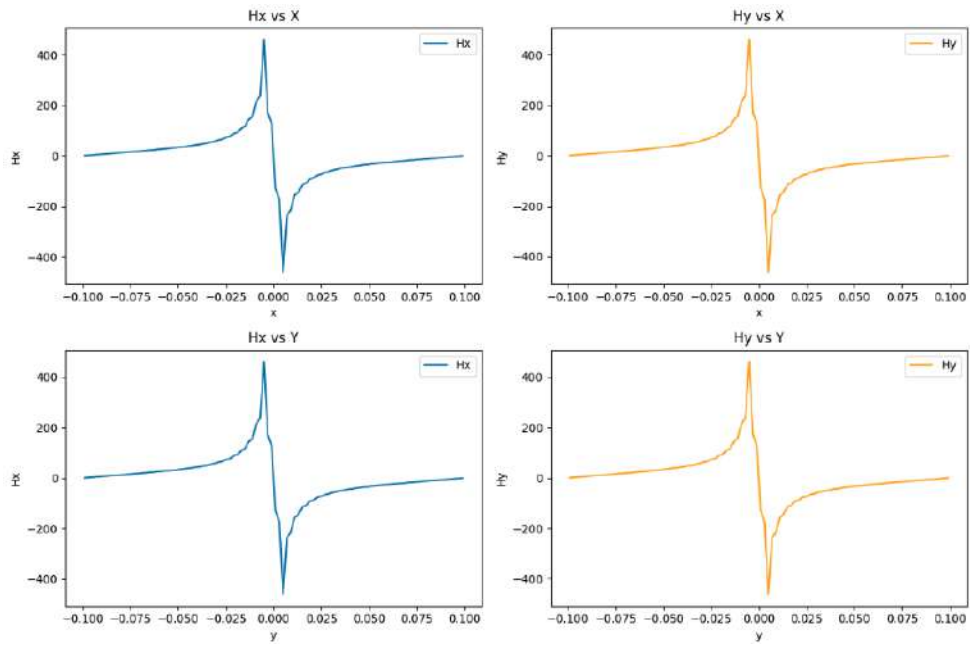Figure 6.5: Diagonal comparison

Figure 6.6: Antidiagonal comparison

7. Current work

We can now use the bond graph to provide an energy representation of a simple system, with discretization based on finite volumes. With a view to describing a transformer, we are currently working on a model consisting of 2 cables placed side by side in a domain composed of air. Both cables have the same geometry and are traversed by a current of identical intensity flowing in the same direction. As in the simple case, we assume that the edge of the domain is far enough from the cables to have a zero magnetic field at the edge.
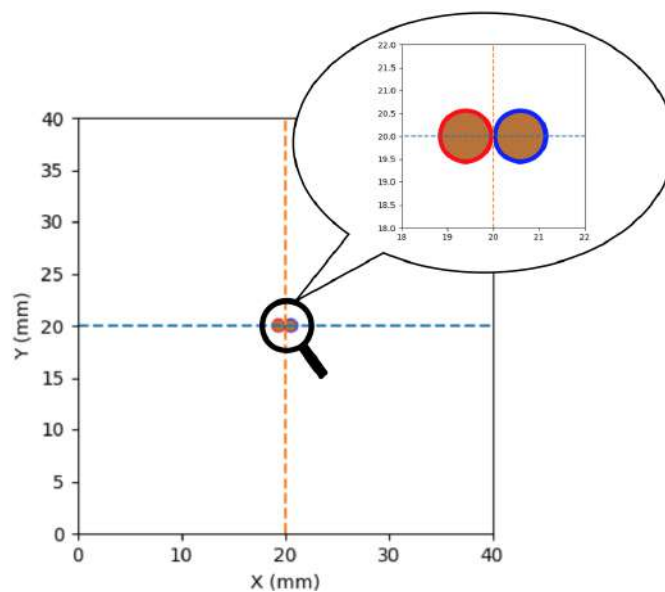

Figure 7.1: Two wires problem

Cables are considered to represent enamelled copper wires. This implies that the copper wire is covered with an insulator. The insulating enamel is applied as a thin layer to the conducting wires, usually copper or aluminum, to insulate them electrically. It is commonly used in the windings of electric motors, transformers, coils and other electromagnetic devices. Enamel ensures that the conductor wire does not short-circuit when wound in several tight layers. It ensures optimum energy efficiency. The enamel chosen in our case is polyimide.

Polyimides are specialty polymers. They have good dielectric properties, high thermal stability and high wear resistance. These good properties are made possible by the fact that they have no melting point or glass transition temperature before decomposition at around 500°C. They offer the best thermal resistance of all enamels.

Our model features are as follows:

➥ Domain $\Omega = 40$ mm $\times$ 40 mm $\times \infty$

➥ Current $I = 2$A (steady, same direction)

➥ Cable diameter $d = 1$ mm

➥ Insulation thickness $e = 0.1$ mm

This problem can be reduced to a two-dimensional one ($\Omega = 40$ mm $\times$ 40 mm). The model will evolve to take account of currents in opposite directions and cables with different diameter or currents. Later, we'll work on a loop.

8. Conclusion

This internship has provided an in-depth exploration of energy representation in systems described by partial differential equations (PDEs), specifically focusing on electromagnetic phenomena. The primary objective was to address the limitations of traditional finite volume methods by integrating them with the bond graph approach, creating a comprehensive model that effectively represents both macroscopic and microscopic characteristics of electromagnetic systems.

Throughout this study, we developed a digital twin of an electromagnetic coupling system, incorporating various modeling techniques and mathematical formulations to capture the complex dynamics of energy transfer. The integration of unstructured mesh techniques within the finite volume method enabled us to accurately represent conservative and diffusive phenomena, thereby overcoming previous modeling challenges. This advancement allows for more precise simulations of low-frequency electromagnetic systems, such as transformers, where minimizing hysteresis losses is critical for enhancing energy efficiency.

The outcomes of this research not only contribute to the field of electrical engineering by providing a novel approach to system modeling but also have practical implications for optimizing transformer design and improving energy conversion efficiency in industrial applications.

Future research could expand on this work by exploring the coupling of thermal and mechanical effects with electromagnetic models to develop even more comprehensive simulations. Additionally, further refinement of the bond graph method and its application to other types of PDE-governed systems could open new avenues for advanced scientific computing and engineering solutions.

Overall, this internship has been a valuable experience that has deepened my understanding of both theoretical and practical aspects of energy representation in complex systems, and it has equipped me with the skills and knowledge to contribute effectively to ongoing advancements in this field.

References

[1] Saba Amirdehi. "Optimisation des modèles électriques du système de traction ferroviaire: Application aux essais virtuels avec l'unité de contrôle". PhD thesis. Institut National Polytechnique de Toulouse-INPT, 2020.

[2] Geneviève Dauphin-Tanguy. *Les Bond Graphs*. Hermes Science Publications, 2000.

[3] Sophie Depeyre. "A stability analysis for finite volume schemes applied to the Maxwell system". In: *ESAIM: Mathematical Modelling and Numerical Analysis* 33.3 (1999), pp. 443–458.

[4] Majid Khalili Dermani and Baptiste Trajin. "System Level Modeling of Electromagnetic Couplings for the Energy Efficiency of Static Converters". In: *2024 IEEE International Conference on Industrial Technology (ICIT)*. 2024, pp. 1–6. DOI: 10.1109/ICIT58233.2024.10540973.

[5] A-S Bonnet-Ben Dhia, Lucas Chesnel, and Patrick Ciarlet Jr. "Two-dimensional Maxwell's equations with sign-changing coefficients". In: *Applied Numerical Mathematics* 79 (2014), pp. 29–41.

[6] David R. Jackson. *Lecture Terms and Definitions*. https://empossible.net/wp-content/uploads/2018/03/Lecture-Terms-and-Definitions.pdf. Accessed: 2024-08-15. 2018.

[7] Majid Khalili Dermani and Baptiste Trajin. "Bond graph methodology for electromagnetic fields simulation in transient and steady state operations". In: *ELECTRIMACS 2024* (2024). Currently in publication.

[8] Stephanie Lohrengel and Malika Remaki. "A FV Scheme for Maxwell's equations". In: *Finite Volumes for Complex Applications III*. Elsevier Science & Technology. 2002, p. 219.

[9] Malika Remaki. "A new finite volume scheme for solving Maxwell's system". In: *COMPEL-The international journal for computation and mathematics in electrical and electronic engineering* 19.3 (2000), pp. 913–932.

[10] Bernard Salamito et al. *Physique tout-en-un MPSI-PTSI*. Dunod, 2013.

A. Python code

```python
import numpy as np
import os
import matplotlib.pyplot as plt
from scipy.interpolate import interp2d

# ----- Define copper color -----
copper_color = '#B87333'

# ----- Domain size -----
domain_size = 0.10

# ----- Cable specifications -----
cable_radius = 0.006
cable_diameter = cable_radius * 2
cable_x0 = 0
cable_y0 = 0

# ----- Density in wire -----
I = 20
A = np.pi * (cable_radius**2)
J_sigma = I / A

# ----- Discretization -----
#dx = 0.001
#dy = 0.001
dx = 0.002
dy = 0.002
x_vector = np.arange(-domain_size, domain_size, dx)
y_vector = np.arange(-domain_size, domain_size, dy)
x_vector += dx/2
y_vector += dy/2
len_x = len(x_vector)
len_y = len(y_vector)

def density(x, y):
    # ----- Distance to cables centers -----
    distance_to_cable = np.sqrt((x - cable_x0)**2 + (y -
    cable_y0)**2)

    # ----- Check spot -----
```

```python
        if distance_to_cable <= cable_radius:
            return J_sigma
    else:
        return 0

# ———— Create a grid for J values ————
J = np.zeros((len_y, len_x))

# ———— Calculate J for each point in the grid ————
for i, x in enumerate(y_vector):
    for j, y in enumerate(x_vector):
        J[i, j] = density(x, y)

inv_dx = 1 / dx
inv_dy = 1 / dy
inv_2dx = 1 / (2*dx)
inv_2dy = 1 / (2*dy)
len_H = len_x * len_y
Hx_vector = np.zeros(len_H)
Hy_vector = np.zeros(len_H)
H_vector = np.zeros(2*len_H)
Assemble_Hx = np.zeros((len_H, len_H))
Assemble_Hy = np.zeros((len_H, len_H))

# ———— Transform J to vector row by row ————
J_vector = J.flatten()

# ———— Assembly matrix A_Hy ————
for j in range(len_y):
    for i in range(len_x):
        if i == 0:
            Assemble_Hy[j*len_x+i, j*len_x+i] = -1
            Assemble_Hy[j*len_x+i, j*len_x+i+1] = 1
        elif i == len_x - 1:
            Assemble_Hy[j*len_x+i, j*len_x+i-1] = -1
            Assemble_Hy[j*len_x+i, j*len_x+i] = 1
        else:
            Assemble_Hy[j*len_x+i, j*len_x+i-1] = -1
            Assemble_Hy[j*len_x+i, j*len_x+i+1] = 1
Assemble_Hy *= inv_2dx

# ———— Assembly matrix A_Hx ————
for j in range(len_y):
    for i in range(len_x):
        if j == 0:
            Assemble_Hx[j*len_x+i, j*len_x+i] = -1
            Assemble_Hx[j*len_x+i, (j+1)*len_x+i] = 1
```

```python
        elif j == len_y - 1:
            Assemble_Hx[j*len_x+i, (j-1)*len_x+i] = -1
            Assemble_Hx[j*len_x+i, j*len_x+i] = 1
        else:
            Assemble_Hx[j*len_x+i, (j+1)*len_x+i] = 1
            Assemble_Hx[j*len_x+i, (j-1)*len_x+i] = -1
Assemble_Hx *= -inv_2dy

# ------ Concatenate A ------
Assemble_H = np.hstack((Assemble_Hy, Assemble_Hx))

# ------ SVD decomposition on dense matrix ------
U, S, VT = np.linalg.svd(Assemble_H, full_matrices=False)

# ------ Pseudo-inverse computation ------
S_inv = np.diag(1 / S)
Assemble_H_pseudo_inv = VT.T @ S_inv @ U.T  # Complete pseudo-
    inverse computation

# ------ Solve equation Ah + j = 0 => h = -A_pseudo_inv @ j ------
H_vector = Assemble_H_pseudo_inv @ J_vector

# ------ Hx and Hy extraction ------
Hy_vector = H_vector[0 : len_H]
Hx_vector = H_vector[len_H :]

# ------ Reshape Hx and Hy in matrix ------
Hx = Hx_vector.reshape((len_x, len_y))
Hy = Hy_vector.reshape((len_x, len_y))

X, Y = np.meshgrid(x_vector, y_vector)

# ------ Create figure ------
plt.figure()

# ------ Plot the cable ------
circle = plt.Circle((0, 0), cable_radius, color=copper_color,
    alpha=1)

# ------ Add cable to the plot ------
ax = plt.gca()
ax.add_patch(circle)

# ------ Plot magnetic field ------
plt.quiver(X, Y, Hx, Hy)

# ------ Set labels ------
```

```python
plt.title('Magnetic field H view')
plt.xlabel('x')
plt.ylabel('y')

# Chemin complet pour enregistrer l'image
save_path = os.path.join(save_dir, 'magnetic_field_Hbc_nul.png')

# Enregistrer l'image
plt.savefig(save_path, bbox_inches='tight', pad_inches=0)

# ―――― figure display ――――
plt.show()
```